Cell

Homeostatic Levels of p62 Control Cytoplasmic Inclusion Body Formation in Autophagy-Deficient Mice

Masaaki Komatsu,[1,2,3] Satoshi Waguri,[4] Masato Koike,[5] Yu-shin Sou,[1,2] Takashi Ueno,[2] Taichi Hara,[6] Noboru Mizushima,[6,7] Jun-ichi Iwata,[1,2] Junji Ezaki,[2] Shigeo Murata,[1] Jun Hamazaki,[1] Yasumasa Nishito,[1] Shun-ichiro Iemura,[8] Tohru Natsume,[8] Toru Yanagawa,[9] Junya Uwayama,[9] Eiji Warabi,[9] Hiroshi Yoshida,[9] Tetsuro Ishii,[9] Akira Kobayashi,[10] Masayuki Yamamoto,[10] Zhenyu Yue,[11] Yasuo Uchiyama,[5] Eiki Kominami,[2] and Keiji Tanaka[1,*]

[1]Laboratory of Frontier Science, Tokyo Metropolitan Institute of Medical Science, Bunkyo-ku, Tokyo 113-8613, Japan
[2]Department of Biochemistry, Juntendo University School of Medicine, Bunkyo-ku, Tokyo 113-8421, Japan
[3]PRESTO, Japan Science and Technology Corporation, Kawaguchi 332-0012, Japan
[4]Department of Anatomy and Histology, Fukushima Medical University School of Medicine, Hikarigaoka, Fukushima 960-1295, Japan
[5]Department of Cell Biology and Neurosciences, Osaka University Graduate School of Medicine, Suita, Osaka 565-0871, Japan
[6]Department of Physiology and Cell Biology, Tokyo Medical and Dental University Graduate School and Faculty of Medicine, Bunkyo-ku, Tokyo 113-8519, Japan
[7]SORST, Japan Science and Technology Corporation, Kawaguchi 332-0012, Japan
[8]National Institutes of Advanced Industrial Science and Technology, Biological Information Research Center (JBIRC), Kohtoh-ku, Tokyo 135-0064, Japan
[9]Graduate School of Comprehensive Human Sciences, University of Tsukuba, Tennoudai, Tsukuba 305-8575, Japan
[10]Department of Medical Biochemistry and ERATO-JST, Tohoku University Graduate School of Medicine, Aoba-ku, Sendai 980-8575, Japan
[11]Departments of Neurology and Neuroscience, Mount Sinai School of Medicine, New York, NY 10029, USA
*Correspondence: tanakak@rinshoken.or.jp
DOI 10.1016/j.cell.2007.10.035

SUMMARY

Inactivation of constitutive autophagy results in formation of cytoplasmic protein inclusions and leads to liver injury and neurodegeneration, but the details of abnormalities related to impaired autophagy are largely unknown. Here we used mouse genetic analyses to define the roles of autophagy in the aforementioned events. We report that the ubiquitin- and LC3-binding protein "p62" regulates the formation of protein aggregates and is removed by autophagy. Thus, genetic ablation of *p62* suppressed the appearance of ubiquitin-positive protein aggregates in hepatocytes and neurons, indicating that p62 plays an important role in inclusion body formation. Moreover, loss of *p62* markedly attenuated liver injury caused by autophagy deficiency, whereas it had little effect on neuronal degeneration. Our findings highlight the unexpected role of homeostatic level of p62, which is regulated by autophagy, in controlling intracellular inclusion body formation, and indicate that the pathologic process associated with autophagic deficiency is cell-type specific.

INTRODUCTION

Macroautophagy (hereafter referred to as autophagy) is a highly conserved bulk protein degradation pathway in eukaryotes. In the initial step of this process, the cytoplasmic portions and organelles are engulfed within a double-membrane vesicle called autophagosome, and then the autophagosome fuses with the lysosomes to degrade the sequestered materials by various lysosomal hydrolytic enzymes, followed by generation of amino acids that are recycled for macromolecular synthesis and energy production. Emerging evidence emphasizes the importance of autophagy in various biological and pathological processes, such as cellular remodeling, tumorigenesis, and developmental programs (Levine and Klionsky, 2004).

Recent evidence indicates that in mammalian cells, autophagy serves two physiological purposes. The first is to supply amino acids for cell survival under poor environmental conditions, which is universally known as "adaptive autophagy." Indeed, this type of autophagy is rapidly induced under nutritional deprivation in yeast (Tsukada and Ohsumi, 1993) and in newborn mice (Kuma et al., 2004), serving as a basic survival strategy in all eukaryotes. The second is to degrade proteins in the cell through continuous operation at a low level irrespective of nutritional stress, known as "basal or constitutive autophagy." In the latter pathway, autophagy is responsible for the

turnover of long-lived proteins, disposal of excess (Iwata et al., 2006) or damaged organelles (Elmore et al., 2001), and clearance of aggregate-prone proteins (Fortun et al., 2003; Kamimoto et al., 2006; Ravikumar et al., 2004). Recent genetic studies using mice have highlighted the importance of constitutive autophagy in nondividing cells, such as hepatocytes and neurons, in which loss of autophagy results in severe liver injury and neurodegeneration, respectively (Hara et al., 2006; Komatsu et al., 2005, 2006). Unexpected findings in these studies were that loss of autophagy causes cytoplasmic accumulation of ubiquitin-positive proteinaceous inclusions, together with hepatocytic and neuronal death without expression of proteins with disease-associated mutations (Hara et al., 2006; Komatsu et al., 2005, 2006). However, the underlying mechanism of inclusion body formation in the aforementioned diseases is largely unknown at present.

Using mouse genetics, we report the critical role of the multifunctional protein "p62/A170/SQSTM1" (also known as a signaling adaptor/scaffold protein) in the formation of intracellular ubiquitin-related protein aggregation caused by deficiency in autophagy. We show that autophagic degradation of the "p62" via direct interaction with LC3, a posttranslational modifier essential for autophagosome formation, prevents inclusion body formation. Importantly, our studies uncover the molecular mechanism linking autophagy, p62, and inclusion body formation, which is a cellular hallmark in various pathophysiological conditions, and reveal pathophysiological changes associated with loss of p62 and/or autophagy in hepatocytes and neurons.

RESULTS

Identification of LC3-Interacting Proteins

The microtubule-associated protein 1A/1B *light chain 3* (LC3) is a modifier protein conjugated with phosphatidylethanolamine (PE), analogous to Atg8 in yeast (Ichimura et al., 2000). PE-conjugated LC3 (LC3-II) is localized in the inner and outer membranes of autophagosomes, and the population associated with the inner membrane is degraded after fusion of autophagosomes with lysosomes (Kabeya et al., 2000). To identify protein(s) that could interact with LC3, we employed the proteomic approach as described previously (Komatsu et al., 2004) and then identified a unique protein p62 as one of LC3-interacting proteins, in addition to LC3-modifying enzymes (Ohsumi, 2001) (Table S1). The p62 protein is conserved in metazoa and plants but not in yeasts and can bind a large number of proteins through its multiple protein-protein interaction motifs (Moscat et al., 2006) (Figure S1). This protein mediates diverse signaling pathways including cell stress, survival, and inflammation (Moscat et al., 2006; Wooten et al., 2006).

p62 Is Degraded by Autophagy-Lysosome Pathway

To verify the interaction between LC3 and p62 in vivo, we first carried out immunoprecipitation assay with cultured hepatocytes isolated from green fluorescent protein (GFP)-LC3 transgenic (Tg) mice (GFP-LC3 tg) (Mizushima et al., 2004) and confirmed the coimmunoprecipitation of p62 with GFP-LC3 under both nutrient-rich and -poor conditions (Figure 1A). We also confirmed the coimmunoprecipitation of p62 with endogenous LC3 in wild-type mouse liver (Figure 1B). In addition to the major band, the minor band detected by our p62 antibody was probably a p62 splicing variant product found in the mouse protein database or a partially cleaved product (see also Figures 2, 3, and 4). Moreover, recombinant p62 was pulled down with recombinant GST-LC3 (Figure 1C), indicating direct physical interaction between p62 and LC3. Subsequent binding assays with a series of recombinant p62 mutants indicated that p62 interacts with LC3 through a linker region that connects the N-terminal Zinc finger and the C-terminal *ubi*quitin-associated (UBA) domain of p62 (Figure S1). Immunofluorescence microscopy using hepatocytes isolated from GFP-LC3 Tg mice showed colocalization of large numbers of punctate signal for GFP-LC3 (84.7% ± 10.9%, ± SD, n = 21) with that for p62 (Figure 1E). When autophagosome formation was induced by nutrient-deprivation, 34.9% ± 6.7% (n = 22) of ring-shaped GFP-LC3-positive autophagosomes contained p62 signal, some of which showed partial colocalization (Figure 1F). A similar colocalization pattern was also observed in liver sections of GFP-LC3 Tg starved for 1 day (Figure 1G). The p62-positive and GFP-LC3-negative particles might correspond to late endosomes or lysosomes, as reported previously (Sanchez et al., 1998). Consistent with the notion that some population of LC3-II is degraded in lysosomes (Kabeya et al., 2000), treatment with lysosomal enzyme inhibitors, but not with a proteasomal inhibitor, resulted in the accumulation of LC3-II in primary hepatocytes (Figure 1D). Similarly, lysosomal inhibition resulted in marked accumulation of p62 (Figure 1D). When lysosomal inhibitors were added to cultured hepatocytes, the majority of p62 accumulated around the perinuclear region, where it colocalized with the lysosomal marker LysoTracker (Figure 1H), suggesting the turnover of p62 together with LC3II in lysosomes.

p62 Is a Component of Inclusions in Autophagy-Deficient Hepatocytes

If p62 is degraded by the autophagic-lysosome pathway, autophagy deficiency should result in the accumulation of p62 protein. To test this in vivo, we used the *Atg7*$^{F/F}$:Mx1 mice, in which *Atg7*, a gene essential for autophagy, can be depleted in the liver by intraperitoneal injections of polyinosinic acid-polycytidylic acid (pIpC) (Figure 2A, left panel) (Komatsu et al., 2005). We observed specific accumulation of p62 protein in *Atg7*-deficient livers (Figures 2A and 2D) without marked induction of p62 mRNA (Figure 2E). Similar to *Atg7* knockout liver, deficiency of *Atg5*, which is essential for autophagosome formation (Mizushima et al., 2001), was also associated with marked accumulation of p62 (Figure S2). These results indicate that p62 turnover is mediated by autophagy. Autophagic

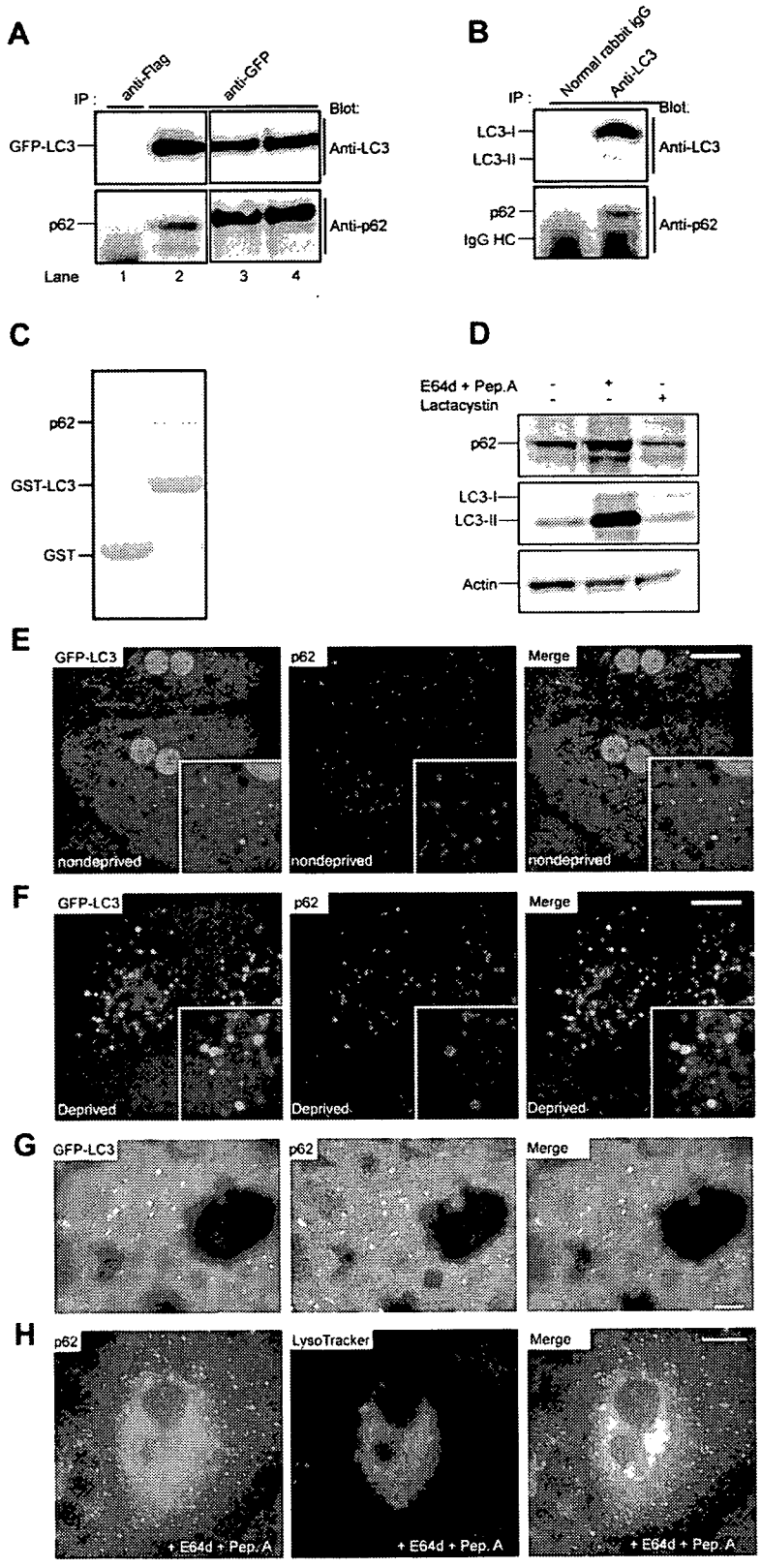

Figure 1. p62 Is Degraded by the Autophagic-Lysosomal Pathway

(A) Interaction of p62 with GFP-LC3. Hepatocytes prepared from GFP-LC3 Tg mice were cultured for 3 hr in Williams' E medium (lanes 1, 2, and 3) or Hank's solution (lane 4). The cell lysates were immunoprecipitated with anti-Flag or GFP antibodies followed by immunoblotting with antibodies against LC3 and p62.

(B) Interaction of p62 with endogenous LC3. Liver lysates from wild-type mice were immunoprecipitated with anti-LC3 antibody or normal rabbit IgG followed by immunoblotting with antibodies against LC3 and p62.

(C) In vitro GST pull-down analysis of purified p62 by recombinant GST or GST-LC3.

(D) Degradation of p62 and LC3. Hepatocytes prepared from wild-type mice were treated with E64d (10 μg/ml) and pepstatin A (10 μg/ml) for 24 hr or lactacystin (10 μM) for 3 hr. The cell lysates were subjected to SDS-PAGE followed by immunoblotting with indicated antibodies. Data shown in (A)–(D) are representative of three separate experiments.

(E, F, and H) Immunofluorescent analysis of primary cultured hepatocytes. Hepatocytes isolated from GFP-LC3 Tg mice were cultured for 3 hr in Williams' E medium (E) and Hank's solution (F) or for 24 hr in Williams' E with E64d and pepstatin A (H) and then immunostained with antibody against p62. Lysosomal inhibitor-treated hepatocytes were stained with the fluorescent acidotropic probe LysoTracker prior to p62 immunostaining (H). Higher magnification views are shown in insets. Bar, 10 μm.

(G) Immunofluorescence analysis of the liver of GFP-LC3 Tg mice. Mice were fasted for 1 day, and then the liver sections were immunostained with anti-p62 antibody. Right panels show merged images. Bar, 10 μm.

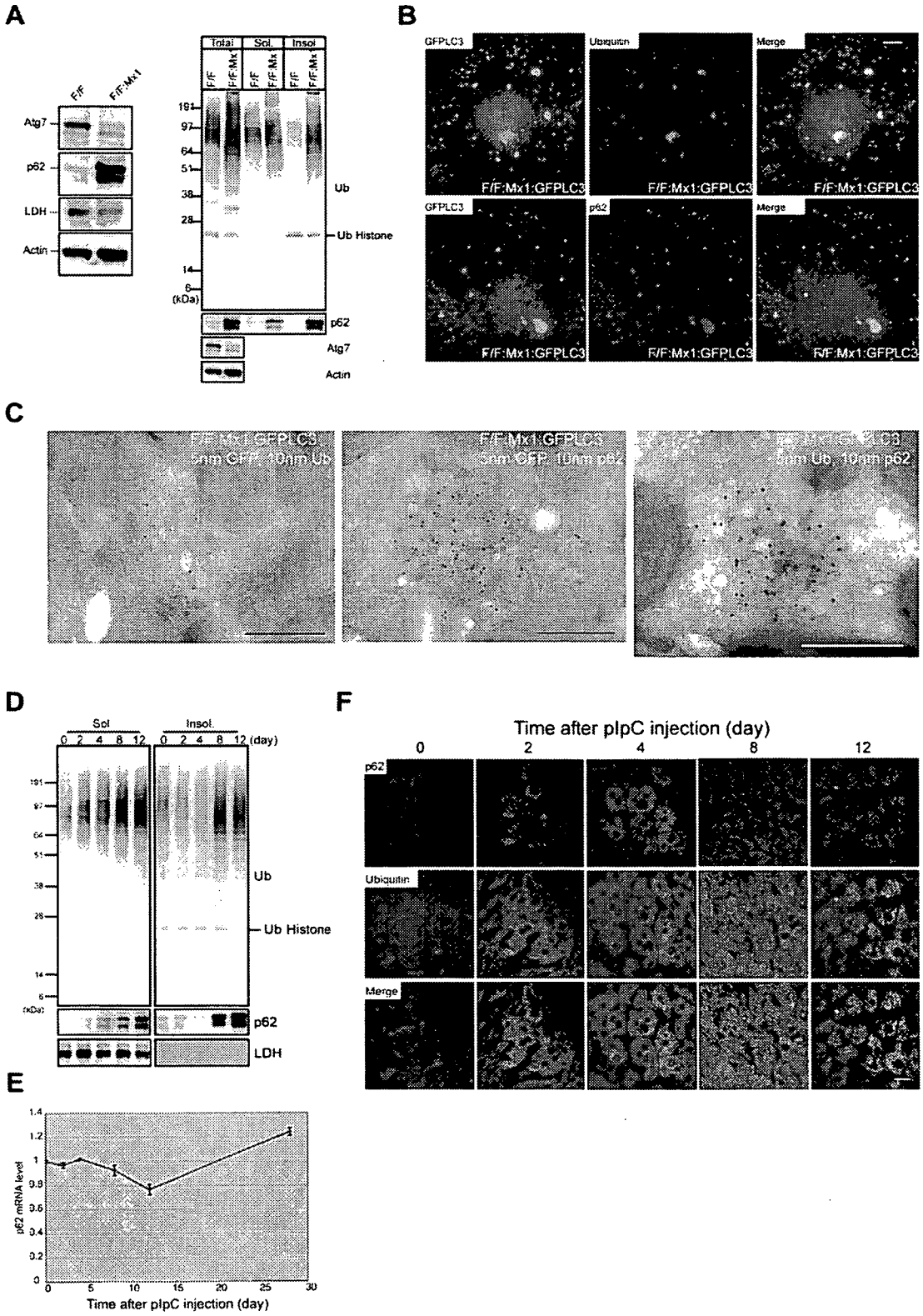

Figure 2. Formation of Ubiquitin- and p62-Positive Inclusions in Autophagy-Deficient Hepatocytes

(A) Accumulation of p62 in *Atg7*-deficient hepatocytes. Left panel shows liver homogenates from *Atg7*$^{F/F}$ and *Atg7*$^{F/F}$:Mx1 mice at 28-day post-pIpC injection were subjected to SDS-PAGE followed by immunoblotting with indicated antibodies. Right panel shows liver homogenates were separated

breakdown of p62 appears to occur irrespective of cell type, because a similar observation was recently reported in HeLa, HEK293T, and mouse embryonic fibroblasts (Bjorkoy et al., 2005; Wang et al., 2006).

Interestingly, abundant amounts of p62 were noted in both detergent-soluble and insoluble fractions from *Atg7*-deficient livers (Figure 2A, right-middle panel), in parallel with accumulation of ubiquitinated proteins in both fractions from *Atg7*-deficient but not from control livers (Figure 2A, right-top panel) (Komatsu et al., 2005). Subsequently, to investigate the cellular localization of ubiquitin, p62, and LC3 in autophagy-deficient hepatocytes, we generated the $Atg7^{F/F}$:Mx1:GFP-LC3 mice by crossing $Atg7^{F/F}$:Mx1 with GFP-LC3 Tg mice. Immunofluorescence microscopy showed that the *Atg7*-deficient cultured hepatocytes contained abundant ubiquitin- (Figure 2B, top panels), or p62- (Figure 2B, bottom panels) positive inclusions in the cytoplasm, which were also positive for GFP-LC3. Finally, double immunoelectron microscopy confirmed the colocalization of LC3, ubiquitin, and p62 proteins in the cytoplasmic aggregated structures (Figures 2C and S3). Next, we analyzed the inclusion formation process. Immunoblot analysis revealed that p62 began to accumulate in the detergent-soluble fraction at 4 days and was abundant in both detergent-soluble and -insoluble fractions at 8 days (Figure 2D). In contrast, RT-PCR analysis showed no induction of p62 transcript during this period (Figure 2E). The accumulation pattern of polyubiquitinated proteins essentially matched that of p62 (Figure 2D). Double-immunofluorescence microscopy showed the appearance of ubiquitin- and p62-double-positive dots at 2 days in some $Atg7^{F/F}$:Mx1 hepatocytes (Figure 2F). At later stages, both the number of hepatocytes containing the inclusions and the size of the inclusions increased gradually with time. These results suggest the time-dependent development of inclusions containing both ubiquitin and p62 in autophagy-deficient hepatocytes.

p62 Is a Component of Inclusions in Autophagy-Deficient Neurons

Next, we investigated the behavior of p62 in neuronal-specific autophagy-deficient mice, $Atg7^{F/F}$:Nes mice (Komatsu et al., 2006). Similar to autophagy-deficient livers, p62 accumulated in the mutant brain without the apparent induction of its mRNA (Figures 3A and 3B), implying a common pathway in p62 turnover across tissues. Furthermore, the p62-positive inclusions were observed immunohistochemically in various brain regions in $Atg7^{F/F}$:Nes mice (Figure S4). Double-immunofluorescence microscopy revealed extensive colocalization of p62 and LC3 (Figure 3C, left panels), or p62 and ubiquitin (Figure 3C, right panels), in numerous inclusions in the cerebral cortex. Immunoelectron microscopy confirmed the localization of p62 in the cytoplasmic aggregated structures (Figures 3D, top panel, and S5). These inclusions also contained ubiquitin (Figures 3D, bottom panel, and S5). Next, we investigated the time course of inclusion formation in the cerebral cortex of $Atg7^{F/F}$:Nes mice from 2 to 28 days after birth. Ubiquitin/p62-double-positive dots began to appear at postnatal day 2 in the cerebral cortex, and they increased in size and number during postnatal development (Figure 3E). Taken together, these results indicate that reduced autophagic activity leads to the formation of ubiquitin- and p62-double positive inclusions in neurons.

Generation of *p62*-Knockout Mice

To examine the physiological roles of p62 in autophagy, we generated *p62*-knockout ($p62^{-/-}$) mice (Figure S6). They were born at Mendelian frequency, fertile and lived longer than 1 year (data not shown). Although *p62* deficiency was associated with adulthood-onset obesity and diabetes as reported recently (Rodriguez et al., 2006), no apparent abnormality was noted in the *p62*-deleted liver (Figure S7). Moreover, *p62*-deficient mice exhibited neither marked neurodegeneration nor inclusion formation in neurons (see Figures 6 and S8). The conversion from LC3-I to LC3-II, induction of GFP-LC3 dots, and the appearance of many autophagosome structures after starvation were similar between the control and *p62*-deficient hepatocytes (Figures S9A, S9B, and S9C). Furthermore, there was no significant change in the turnover of long-lived protein in the mutant hepatocytes (Figure S9D).

into detergent (0.5% Tx-100)-soluble (Sol.) and insoluble (Insol.) fractions. Each fraction was subjected to SDS-PAGE and analyzed by immunoblotting with indicated antibodies. Data shown are representative of three separate experiments.

(B) Immunofluorescence analysis of cellular localization of ubiquitin, p62, and LC3 in autophagy-deficient hepatocytes. Hepatocytes isolated from $Atg7^{F/F}$:Mx1:GFP-LC3 mice at 14-day post-pIpC injection were immunostained with anti-ubiquitin or p62 antibodies. Right panels show merged images. Bar, 10 μm.

(C) Immunoelectron micrograph showing double labeling of ubiquitin (10 nm colloidal gold particles [cgp]) and GFP (5 nm cgp), p62 (10 nm cgp), and GFP (5 nm cgp), or p62 (10 nm cgp) and ubiquitin (5 nm cgp) in hepatocytes isolated from $Atg7^{F/F}$:Mx1:GFP-LC3 mice at 14-day post-pIpC injection. Bars, 0.5 μm. Magnified images can be seen in Figure S3.

(D) Immunoblotting analyses of ubiquitinated proteins and p62 in $Atg7^{F/F}$:Mx1 mice livers at various time points post-pIpC injection. Each fraction prepared as shown in (A) was subjected to SDS-PAGE and analyzed by immunoblotting with indicated antibodies. Data shown are representative of three separate experiments.

(E) Quantitation of p62 mRNA level in $Atg7^{F/F}$:Mx1 liver by RT-PCR. Total RNAs were prepared from $Atg7^{F/F}$:Mx1 livers at various time points post-pIpC injection, and then cDNA was synthesized from each RNA, followed by real-time PCR analysis. Data are mean ± standard deviation (SD) values of p62 mRNA normalized to the amount in $Atg7^{F/F}$:Mx1 liver at 0 day post-pIpC injection.

(F) Immunohistochemical detection of p62- and ubiquitin-positive inclusions in *Atg7*-deficient livers. $Atg7^{F/F}$:Mx1 mice were sacrificed at various time points post-pIpC injection, and liver sections were immunostained with anti-ubiquitin and p62 antibodies. Bottom panels show merged images. Bar, 10 μm.

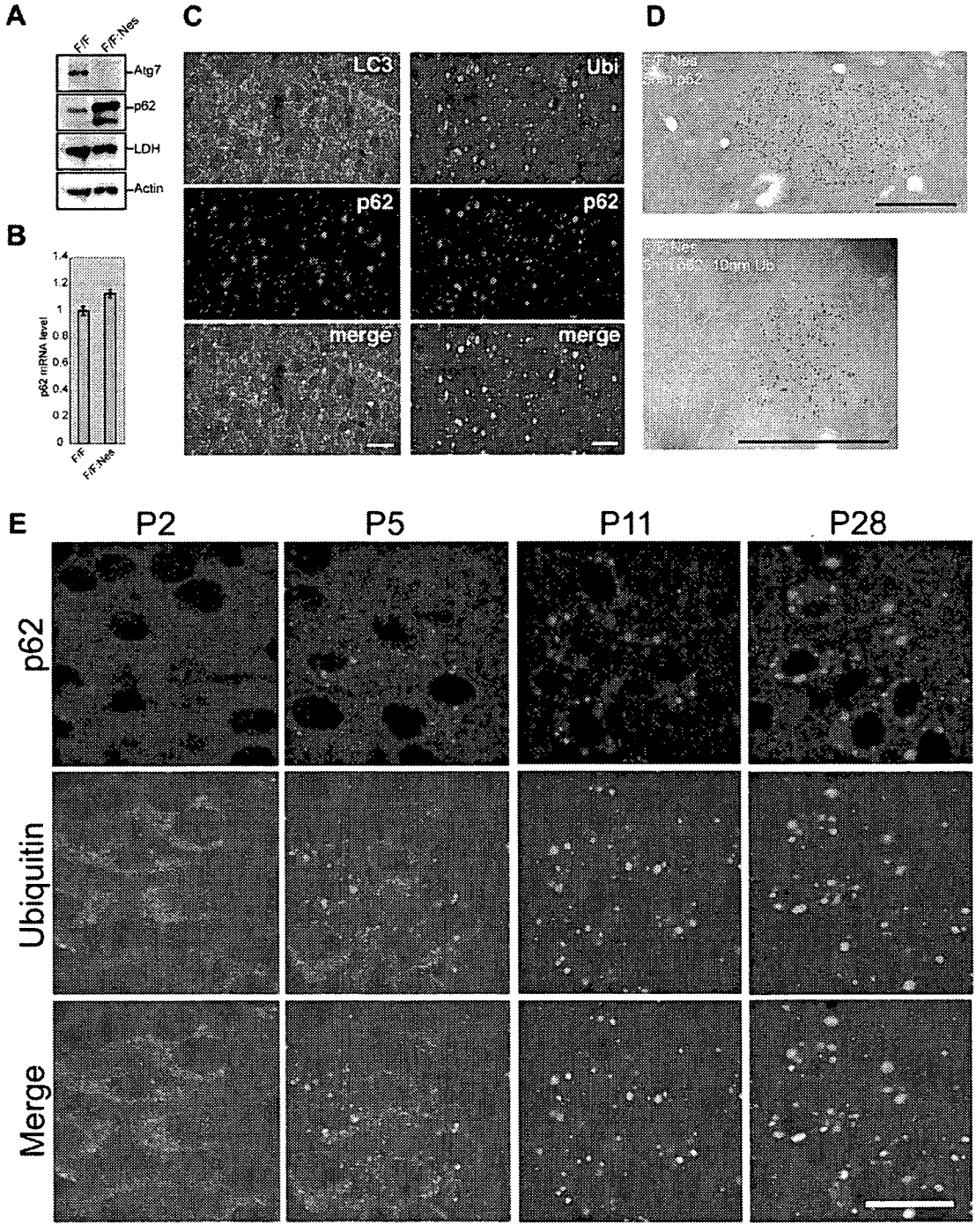

Figure 3. Formation of Ubiquitin- and p62-Positive Inclusions in Autophagy-Deficient Neurons

(A) Accumulation of p62 in *Atg7*-deficient brains. Brain homogenates from *Atg7*$^{F/F}$ and *Atg7*$^{F/F}$:Nes mice at 8 weeks of age were subjected to SDS-PAGE and analyzed by immunoblotting with indicated antibodies. Data shown are representative of three separate experiments.

(B) Quantitation of p62 mRNA level in *Atg7*-deficient brains by RT-PCR. Total RNAs were prepared from brains of *Atg7*$^{F/F}$ and *Atg7*$^{F/F}$:Nes mice at 8 weeks of age and analyzed as shown in Figure 2E. Data are mean ± SD values of p62 mRNA normalized to the amount in *Atg7*$^{F/F}$ brain. The experiments were performed three times.

(C) Immunofluorescence microscopy in *Atg7*$^{F/F}$:Nes cerebral cortex. Brain sections of *Atg7*$^{F/F}$:Nes mice were immunostained with anti-LC3 and p62 antibodies (left panels) or anti-ubiquitin and p62 antibodies (right panels). Bottom panels show merged images. Bar, 10 μm.

(D) Immunoelectron micrograph showing labeling of p62 (top panel) or double labeling of ubiquitin (10 nm cgp) and p62 (5 nm cgp) in hypothalamic neurons of 8-week-old *Atg7*$^{F/F}$:Nes mice. Bars, 0.5 μm. Magnified images can be seen in Figure S5.

Loss of p62 Suppresses Inclusion Formation in Autophagy-Deficient Hepatocytes

Next, to investigate the roles of p62 in inclusion formation, we crossed *Atg7*$^{F/F}$:Mx1 with *p62*$^{-/-}$ mice, producing the *Atg7*- and *p62*-double knockout (DKO) mice (*Atg7*$^{F/F}$:Mx1:*p62*$^{-/-}$). In contrast to large number of inclusions positive for ubiquitin in *Atg7*-deficient hepatocytes, surprisingly such ubiquitin inclusions were almost completely dispersed in the DKO hepatocytes (Figure 4A). Immunoblot analysis revealed that the amounts of accumulated polyubiquitinated proteins in DKO liver were lower than those in *Atg7*-deficient liver. Moreover, the reduction was more prominent in the insoluble fraction (Figures 4B and S10A). Interestingly, proteasome function evaluated by the degradation of polyubiquitinated protein was not significantly different among the genotypes (Figure S11A). Furthermore, the degradation of long-lived protein in DKO hepatocytes was significantly reduced to the levels as shown in *Atg7*-deficient hepatocytes (Figure S11C). Electron microscopic analysis showed that the number of aggregate structures and aberrant concentric membranous structures that were typical in *Atg7*-deficient hepatocytes (Komatsu et al., 2005) were markedly reduced, whereas smooth endoplasmic reticulum and peroxisomes were still abundantly observed in DKO hepatocytes (Figure 4C).

Loss of p62 Suppresses Inclusion Formation in Autophagy-Deficient Neurons

We also examined the roles of p62 in inclusion formation in autophagy-deficient neurons. As shown in Figure S8, while no ubiquitin-positive inclusions were detected in the brains of wild-type and *p62*-knockout mice, ubiquitin-positive inclusions of various sizes were recognized immunohistochemically in several regions of the *Atg7*$^{F/F}$:Nes brain. Such inclusions were hardly detected in the *Atg7*$^{F/F}$:Nes:*p62*$^{-/-}$ (DKO) neurons (Figures 4D and S8). Unlike autophagy-deficient livers, it was difficult to convincingly detect by immunoblot analyses any differences in the amount of insoluble polyubiquitinated protein between *Atg7*- and *Atg7/p62*-DKO brain (Figures 4E and S10B). This discrepancy could be due to the relatively low amounts of insoluble ubiquitinated proteins in total brain lysates from *Atg7*$^{F/F}$:Nes mice, which were insufficient for the detection of the difference. Actually, the inclusions were observed in some restricted areas such as the hypothalamus and cerebral cortex, and they were hardly observed in glial cells (Hara et al., 2006; Komatsu et al., 2006). Previous electron microscopic analysis showed that the hypothalamic neurons in *Atg7*$^{F/F}$:Nes brain contained large inclusion bodies in the perikarya (Komatsu et al., 2006). Although such inclusions were hardly detected in the same region of DKO brain, we noticed the presence of several large neuritic structures with numerous pleomorphic features of smooth endoplasmic reticulum (Figure 4F; c, e, and f). Similar alteration was also observed in the *Atg7*$^{F/F}$:Nes hypothalamus (Figure 4F, b and d), but not in the control (Figure 4F, a). In the cerebellar nuclei of both *Atg7*$^{F/F}$:Nes and DKO brains, which contained abundant round eosinophilic structures as evident in hematoxylin and eosin (H&E) stained sections (Figure 6C, bottom panel), myelinated axons were frequently enlarged and contained aberrant membranous structures and/or degenerated materials (Figures S12B–S12F), suggesting axonal degeneration in both *Atg7*$^{F/F}$:Nes and DKO neurons. Taken together, these results strongly suggest that the inclusion formation but not axonal degeneration is largely dependent on the presence of p62 in autophagy-deficient neurons.

Liver Injury in Autophagy-Deficient Mice Is Suppressed by Loss of p62

To examine whether abnormalities in autophagy-deficient liver are partly caused by the accumulation of p62, we examined the phenotypes of *Atg7*$^{F/F}$:Mx1:*p62*$^{-/-}$ mice. Surprisingly, simultaneous loss of *Atg7* and *p62* in the liver significantly suppressed the deleterious phenotypes caused by ablation of autophagy (Figures 5A and 5B). Indeed, histological analysis showed hepatocytic hypertrophy in *Atg7*-deficient liver and its suppression in DKO liver. Accordingly, the hepatic lobular structure was considerably better recognized in DKO than in *Atg7*-deficient liver (Figure 5C). While serum levels of aspartate aminotransferase (AST), alanine aminotransferase (ALT), and alkaline phosphatase (ALP) were elevated in the DKO mice compared with the control mice, the levels were markedly lower than those in single *Atg7*-deficient mice (Figure 5D). Almost the same results were observed in *Atg7*$^{F/F}$:Alb:*p62*$^{-/-}$ mice, which exhibited impaired autophagy in hepatocytes at postnatal stage, without pIpC injection (Figure S13), indicating that pIpC injection itself does not affect phenotypes of *Atg7*$^{F/F}$:Mx1 or *Atg7*$^{F/F}$:Mx1:*p62*$^{-/-}$ mice. Taken together, these results indicate that excess accumulation of p62 is a major cause of the pathogenic changes seen in the liver of autophagy-deficient mice.

Ablation of *p62* Leads to Neither Improvement nor Exacerbation of the Phenotypes in Autophagy-Deficient Neurons

Further, to investigate whether defects in autophagy-deficient brain are also attributed to accumulation of p62 in neurons, we examined the phenotypes of *Atg7*$^{F/F}$:Nes:*p62*$^{-/-}$ mice. In contrast to the recovery of liver injury in *Atg7*$^{F/F}$:Mx1 mice by simultaneous loss of *p62*, ablation of *p62* did not rescue behavioral abnormalities such as tremor and abnormal limb clasping recognized in *Atg7*$^{F/F}$:Nes mice (data not shown). Furthermore, histological

(E) Appearance of p62- and ubiquitin-positive inclusions in *Atg7*-deficient cerebral cortex during postnatal (P) development. *Atg7*$^{F/F}$:Nes mice were sacrificed at P2, 5, 11, and 28 days, and the brain sections were immunostained with anti-ubiquitin and p62 antibodies. Bottom panels show merged images. Bar, 20 μm.

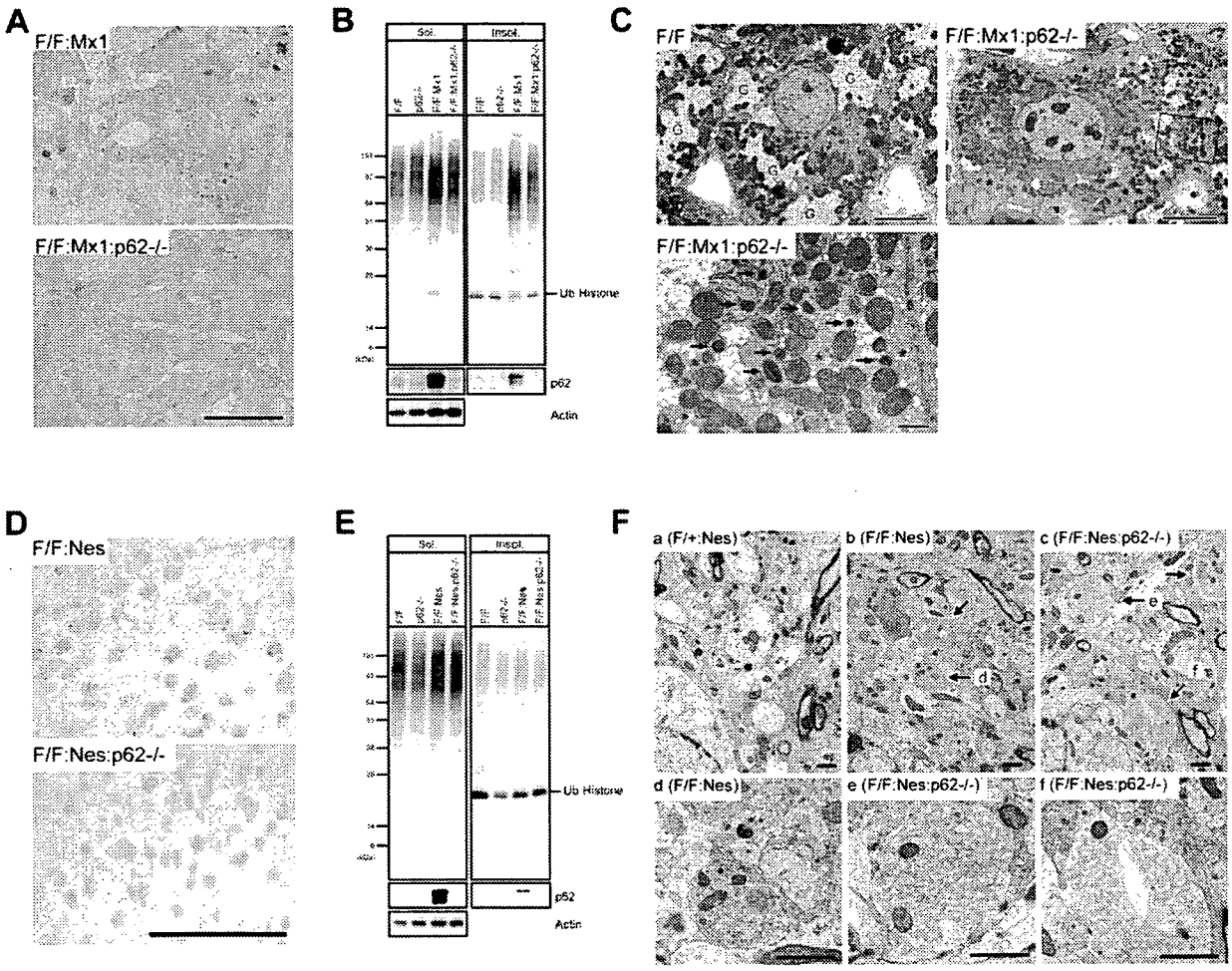

Figure 4. Indispensable Role of p62 in Inclusion Formation in Autophagy-Deficient Cells

(A) Immunohistochemical analysis of ubiquitin inclusions in *Atg7*- and *Atg7/p62*-deficient liver. Liver sections from *Atg7*$^{F/F}$:Mx1 and *Atg7*$^{F/F}$:Mx1:*p62*$^{-/-}$ mice at 14-day post-pIpC injection were immunostained with anti-ubiquitin antibody. Bar, 100 μm.

(B) Immunoblotting analysis of *Atg7*- and *Atg7/p62*-deficient livers. Liver homogenates from mice of the indicated genotype at 28-day post-pIpC injection were separated into detergent-soluble and insoluble fractions as shown in Figure 2. Each fraction was subjected to SDS-PAGE and analyzed by immunoblotting with indicated antibodies. Data shown are representative of three separate experiments.

(C) Electron micrographs of control and *Atg7/p62*-deficient liver. Note that the glycogen area (G), easily observed in control hepatocytes, is markedly reduced in *Atg7/p62*-deficient hepatocytes. The boxed region in the top right panel is further magnified in the bottom left panel. Asterisks indicate regions filled with smooth endoplasmic reticulum. Arrows indicate peroxisomes. Bars, 10 μm (left and right top panels) and 1 μm (left bottom panel).

(D) Immunohistochemical analysis of *Atg7*- and *Atg7/p62*-deficient brains. The presence of ubiquitin-positive particles was examined immunohistochemically in the hypothalamic regions of *Atg7*$^{F/F}$:Nes and *Atg7*$^{F/F}$:Nes:*p62*$^{-/-}$ mice. Bar, 100 μm.

(E) Immunoblotting analysis of *Atg7*- and *Atg7/p62*-deficient brains. Brain homogenates from mice of the indicated genotypes at 8 weeks of age were analyzed by immunoblotting as shown in (B). Data shown are representative of three separate experiments.

(F) Electron micrographs of the hypothalamus of mice of the indicated genotype. Note that several electron-lucent neuritic structures are detected in the control neuropil (a), which are only rarely seen in the *Atg7*- (b) and *Atg7/p62*-deficient (c) tissues. Instead, the latter tissues contain large neurites filled with pleomorphic features of smooth endoplasmic reticulum. Arrows indicate abnormal neuritic structures, some of which are magnified in d, e, and f. Bars, 1 μm.

analyses clearly revealed the lack of Purkinje cells in the cerebellum (Figure 6C) and large pyramidal neurons in both the cerebral cortex (Figure 6A) and hippocampus (Figure 6B) of *Atg7*$^{F/F}$:Nes:*p62*$^{-/-}$ as well as *Atg7*$^{F/F}$:Nes mice. We also found a number of eosinophilic spheroids in H&E-stained sections in the cerebellar nuclei of *Atg7*$^{F/F}$:Nes:*p62*$^{-/-}$ mice, similar to *Atg7*$^{F/F}$:Nes mice (Figure 6C). A marked increase in the number of TUNEL (terminal deoxynucleotidyl transferase [TdT]-mediated dUTP-biotin nick end labeling)-positive cells, which were noted in both *Atg7*$^{F/F}$:Nes cerebral cortices and granular cell layers of the cerebellum at P28, tended to decrease in similar regions of *Atg7*$^{F/F}$:Nes:*p62*$^{-/-}$ mice (Figures 6D and 6E), albeit statistically insignificant. Thus, these results indicate that ablation of *p62* does not result in improvement or exacerbation of the phenotypes in autophagy-deficient neurons.

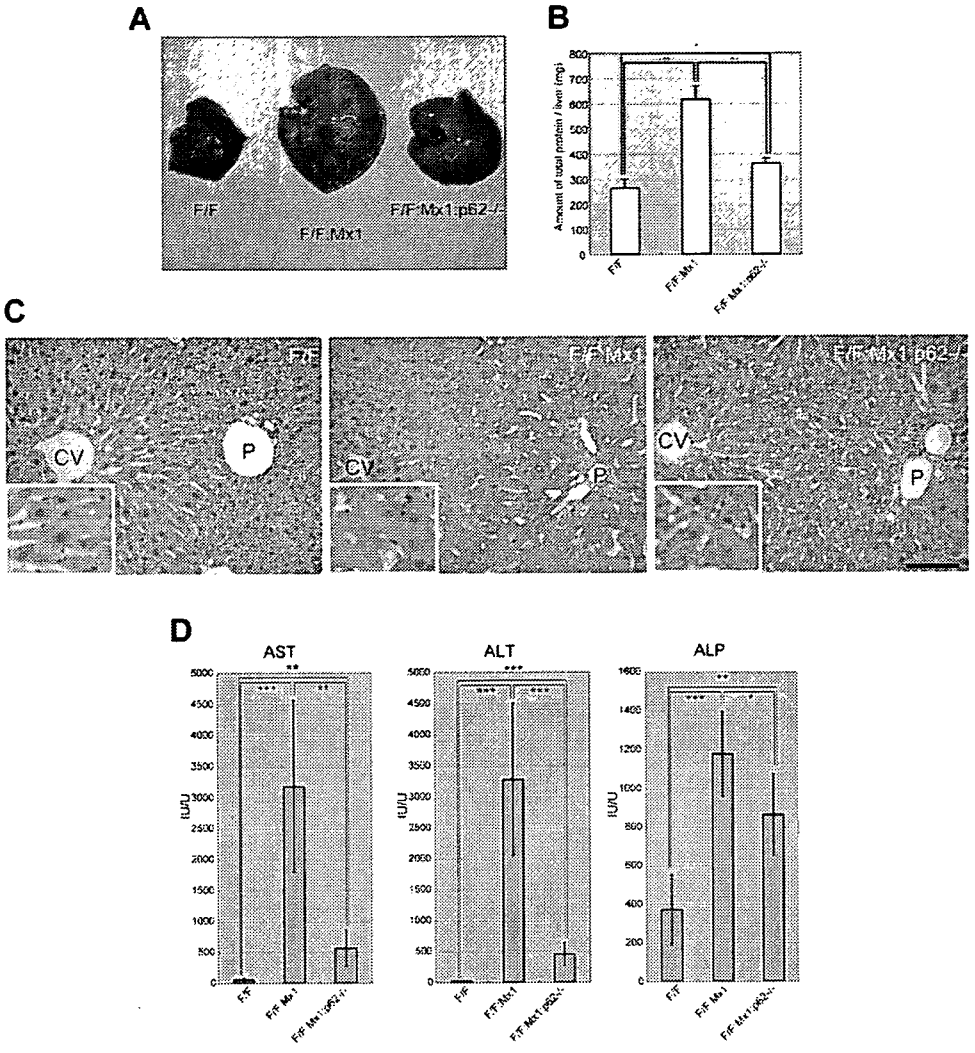

Figure 5. Suppression of Liver Dysfunction in Autophagy-Deficient Mice by Additional Loss of *p62*

(A) Gross anatomical views of representative livers from mice of the indicated genotype at 28-day post-pIpC injection.

(B) Amount of total liver protein. Livers from mice shown in (A) were dissected out, and amounts of total protein per liver were measured. Data are mean ± SD values of five mice in each group. $^{*}p < 0.05$, $^{**}p < 0.01$, and $^{***}p < 0.001$ (Student's t test).

(C) Typical histology of livers from mice of the indicated genotype. H&E staining of respective livers was conducted at 56-day post-pIpC injection. Higher magnification views are shown in insets. CV, central vein; P, portal vein. Bar, 100 μm.

(D) Liver function tests of mice shown in (A). Serum levels of AST, ALT, and ALP were measured. Data represent mean ± SD values of seven mice in each group. $^{*}p < 0.05$, $^{**}p < 0.01$, and $^{***}p < 0.001$.

Aberrant Accumulation of p62 Induces Detoxifying Enzymes in Livers but Not in Brains

Our data clearly showed that loss of *p62* suppresses liver dysfunction but not neurodegeneration in autophagy-deficient mice. How does p62 function differently in autophagy-deficient liver and brain? To elucidate the underlying mechanism for the difference, we examined gene-expression profiles in autophagy-deficient mice by microarray analyses and found that detoxifying enzymes including glutathione S-transferase (GST) families, cytochrome P450 families, and NAD(P)H dehydrogenase quinone 1 (Nqo1) were highly expressed in the autophagy-deficient liver. However, none of these detoxifying enzymes was upregulated in the autophagy-deficient brain (Figure 7A). Moreover, such induction in the liver was suppressed almost completely by additional loss of *p62* (Figure 7A). As shown in Figure 2D, accumulation and insolubilization of both p62 and ubiquitinated proteins began at 4 days post-pIpC injection in $Atg7^{F/F}$:Mx1 liver. Furthermore, upregulation of detoxifying enzymes began at 8 days and reached a plateau at 12 days post-pIpC injection (Figure 7B). Meanwhile, significant leakage of ALT and AST, representing hepatocyte death, occurred at later time points (Figure 7C), suggesting that the increase of detoxifying enzymes was not a secondary effect of liver dysfunction.

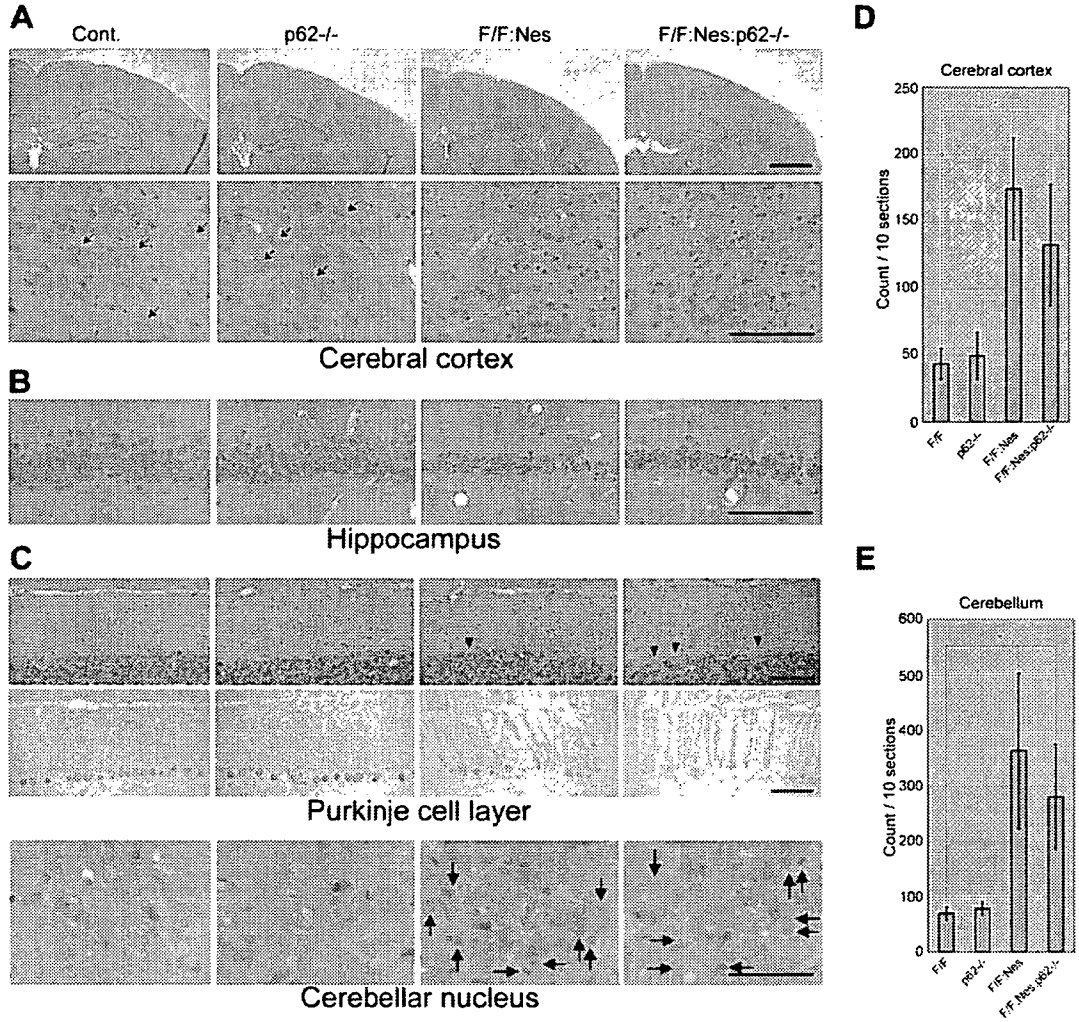

Figure 6. Ablation of *p62* Leads to Neither Improvement nor Exacerbation of the Phenotypes in Autophagy-Deficient Neurons

(A and B) H&E staining of the cerebral cortex (A) and pyramidal cell layer of the hippocampus (B) in mice of the indicated genotype at 4 weeks of age. Top panels in (A) are magnified in bottom panels. Arrows in (A) point to large pyramidal neurons in the cerebral cortex.

(C) Histological analysis of the cerebellar cortex (top and middle panels) and cerebellar nucleus (bottom panel). Cryosections from 8-week-old mice were stained with H&E (top and bottom panels) or immunostained with Purkinje cell marker, calbindin (middle panels). Bars, 1 mm (A, top panel), 200 μm (C, bottom panel), 100 μm (A, bottom panel), (B and C, top and middle panels).

(D and E) Apoptotic cells in the cerebral cortex (D) and cerebellum (E) at 8 weeks of age of the indicated four genotypes. Bars represent the average number (±SD) of total TUNEL-positive cells in ten sections counted in three animals for each genotype. $^*p < 0.05$.

A key question is how such enzymes are specifically induced in the autophagy-deficient liver. To this end, we examined the behavior of the transcriptional factor "Nrf2," which translocates to the nucleus in response to oxidative and electrophilic stresses to activate the transcription of various detoxifying enzymes including Gstm1 and Nqo1 (Tong et al., 2006). As shown in Figure 7D, the level of Nrf2 was markedly higher in the nuclear fraction from *Atg7*$^{F/F}$:Mx1 liver but very low in those from control and *p62*-knockout livers. Importantly, the translocation of Nrf2 into the nucleus in *Atg7*$^{F/F}$:Mx1 liver was almost completely suppressed by additional loss of *p62*, implying that autophagy-deficiency causes cellular stress in the liver, which negatively affects hepatocyte function and concomitantly induces p62-dependent activation of Nrf2.

DISCUSSION

p62 Handles Formation of Cytoplasmic Inclusions

While there is ample evidence that dysfunction of the ubiquitin-proteasome system leads to the formation of ubiquitin-positive inclusions, which are the pathological hallmark of various neurodegenerative diseases (Goldberg, 2003), suppression of autophagy also leads to the formation of ubiquitin-positive inclusion (Hara et al., 2006; Komatsu et al., 2005, 2006). However, the molecular mechanism(s) involved in the formation of these inclusions is not clear to

date. In the present study, we found marked accumulation of p62 and ubiquitinated proteins and subsequent inclusion formation in *Atg7*-deficient mice (Figures 2 and 3). Intriguingly, p62 has been identified as a major component of ubiquitin-containing inclusions known as the "hepatocytic Mallory body" found in alcoholic hepatitis and steatohepatitis (Stumptner et al., 2002). Similar inclusions have been also recognized frequently in proteinaceous aggregates in the remnant neurons in various neurodegenerative disorders such as Parkinson's disease and amyotrophic lateral sclerosis (Kuusisto et al., 2001; Nakano et al., 2004). In such diseases, it is plausible that the reduced autophagic activity may be associated with the generation of inclusion bodies.

Surprisingly, loss of *p62* was associated with marked reduction of ubiquitin-positive inclusions, which were otherwise abundantly present in *Atg7*-deficient hepatocytes and neurons (Figure 4). Because ubiquitin-tagged proteins are sticky but do not exhibit aggregation-prone nature themselves, the high levels of p62 due to impaired autophagy might predispose to inclusion formation via the PB1 domain, which retains the ability of self oligomerization (Lamark et al., 2003). Indeed, overexpression of p62 forms inclusions, which is dependent on the presence of both PB1 and UBA domains (Bjorkoy et al., 2005). Since almost all inclusions in autophagy-deficient cells were positive for both ubiquitin and p62, it is possible that ubiquitinated proteins initially interact with p62, and subsequently the protein complex becomes inclusions in a p62-dependent manner. Although autophagy is involved in protection from several discrete diseases (Fortun et al., 2003; Kamimoto et al., 2006; Ravikumar et al., 2004), whether p62 is indeed essential for the formation of disease-related inclusions or not remains unknown at present. However, intriguingly, the formation of ubiquitin-positive aggregates induced by proteasome inhibition is greatly suppressed in *p62*-deficient cells (Wooten et al., 2006), suggesting that p62 is a general mediator of inclusion formation.

p62-Dependent Liver Impairment in Autophagy-Deficient Mice

Our present studies suggest that the pathological changes in *Atg7*-deficient liver are due, at least in part, to oxidative stress associated with proteinaceous aggregates formed by excess accumulation of p62 and ubiquitinated proteins. However, emerging evidence indicates that protein aggregates containing disease-related proteins (e.g., polyQ) can provide protection (Arrasate et al., 2004; Ross and Poirier, 2005; Sanchez et al., 2003). Similarly, aggregate formation mediated by p62 seems to be a protective mechanism in the presence of overexpression of polyQ (Bjorkoy et al., 2005). Therefore, p62 might play an important role in the surveillance of protein abnormalities by adaptively segregating ubiquitin-tagged toxic proteins as inclusions in cells. It is noteworthy that oligomer and protofibrillar intermediates, which are cytotoxic (Arrasate et al., 2004; Ross and Poirier, 2005; Sanchez et al., 2003), must form before the formation of harmless aggregates and generate reactive oxygen species, which are the primary mediators of oxidative stress (Tabner et al., 2005). Because genetic ablation of autophagy in the liver causes exhaustive accumulation of both p62 and ubiquitinated proteins, the liver might show mixed symptoms related to the cytotoxic effects and protective reactions—i.e., continuous formation of both "harmful oligomer and protofibrillar intermediates" and "harmless aggregates" and induction of both "oxidative stress" and "detoxifying enzymes." According to this scenario, simultaneous loss of p62 under autophagy-deficient background might attenuate accumulation of unfavorable harmful oligomer and protofibrillar intermediates, which ultimately form harmless inclusion, leading to alleviation of liver injury.

In this context, we found that impairment of liver autophagy led to nuclear translocation of Nrf2 (Figure 7D), which is responsible for inducible transcription of various antioxidant and detoxifying enzymes, providing mechanistic insights into the upregulation of those enzymes in the autophagy-deficient liver. In the absence of stress, Nrf2 is constitutively degraded through the ubiquitin-proteasome pathway, since the binding partner Keap1 is a ubiquitin-protein ligase. Exposure to oxidative and electrophilic insults results in modification of Cys residues of Keap1, and leads to inactivation of Keap1. Stabilization of Nrf2 leads to its nuclear translocation to induce the transcription of detoxifying enzymes (Tong et al., 2006). Accordingly, we surmise that the autophagy-deficient liver may be filled with oxidative and/or other Nrf2-inducing stresses. More interestingly, simultaneous loss of *p62* and *Atg7* completely suppressed the translocation of Nrf2 (Figure 7D). These results strongly argue for accumulation of cellular stress in autophagy-deficient liver, the extent of which depends on the impairment of p62 turnover, and they shed light on the mechanism of p62 loss-associated attenuation of autophagy-deficiency-related liver injury.

On the other hand, leakage of hepatocytic enzymes into peripheral blood still occurred at a significantly high level in $Atg7^{F/F}$:Mx1:$p62^{-/-}$ compared with control mice (Figure 5D), implying other abnormalities apart from p62 accumulation in the DKO livers. In fact, in addition to accumulation of soluble ubiquitinated proteins, impairment of organelle turnover was not rescued by the additional defect of *p62* (Figures 4B and 4C). Such abnormalities together with the excess accumulation of p62 might have irreversible cytotoxic effects in autophagy-deficient hepatocytes.

p62-Independent Neuronal Death in Autophagy-Deficient Mice

Unlike the liver, the survival of *Atg7*-deficient neurons is affected little when *p62* is abolished, although p62 can form protein aggregates in neuronal cells as in hepatocytes. This paradoxical observation may underlie the difference in autophagic activity among cell-types or tissues. The constitutive autophagic activity in the brain is low compared

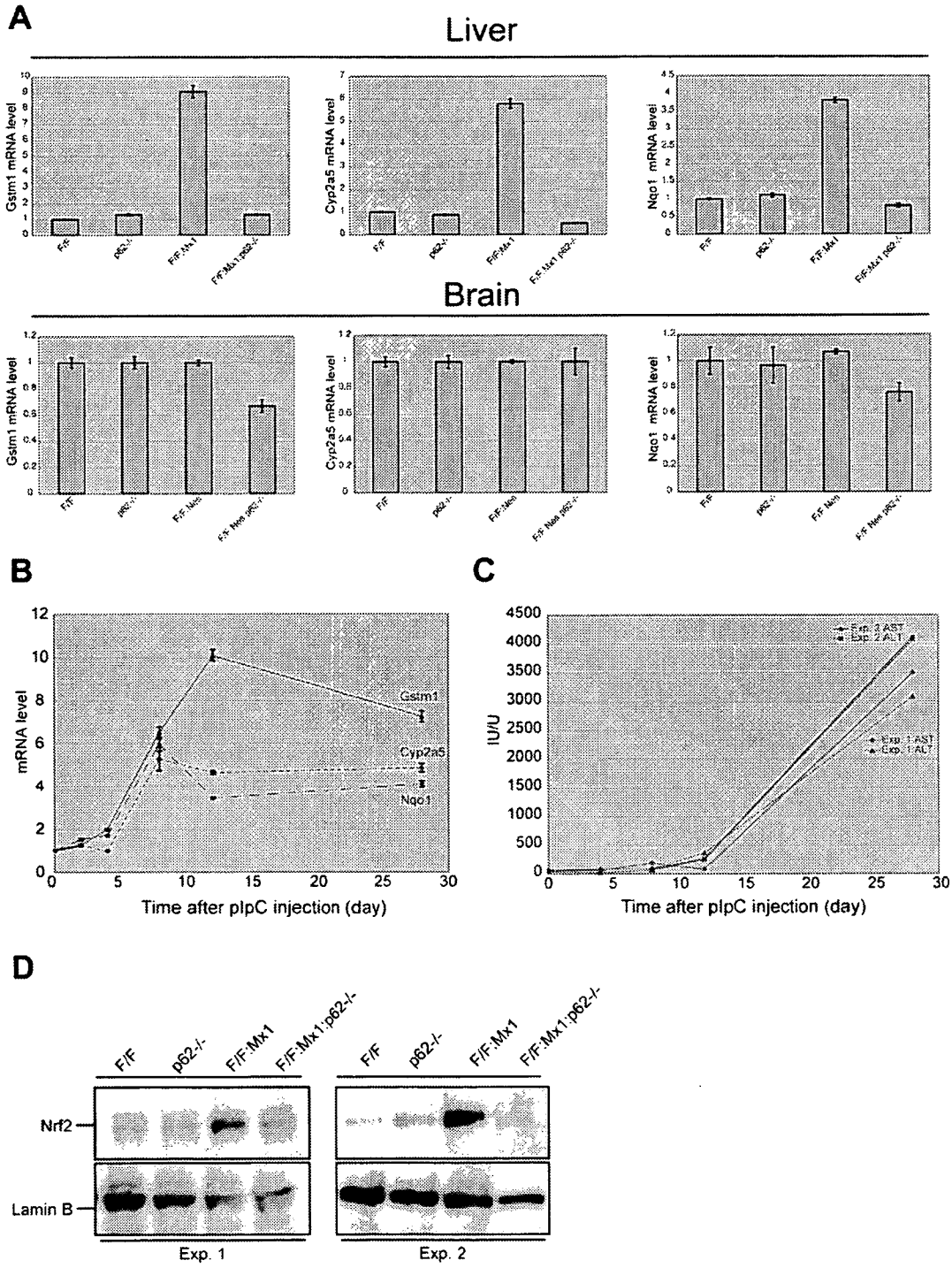

Figure 7. p62-Dependent Induction of Detoxifying Enzymes in Autophagy-Deficient Liver but Not in Brain

(A) Quantitative RT-PCR analyses of Gstm1, Cy2a5, and Nqo1 in mouse liver (top panels) and brain (bottom panels). Total RNAs were prepared from the livers of the indicated genotypes at 12 days post-pIpC injection and brains of the indicated genotypes at postnatal day 28. The values are normalized to the amount of mRNA in $Atg7^{F/F}$ liver and brain. The experiments were performed three times.

(B) Quantitation of mRNA levels of detoxifying enzymes in $Atg7^{F/F}$:Mx1 liver by RT-PCR. Total RNAs were prepared from $Atg7^{F/F}$:Mx1 mice livers at various time points post-pIpC injection, and then cDNA was synthesized from each RNA, followed by real-time PCR analyses. The values are normalized to the amount of each mRNA in $Atg7^{F/F}$:Mx1 liver at 0 days post-pIpC injection.

(C) Liver function tests of mice at various time points post-pIpC injection. Serum levels of AST and ALT were measured in $Atg7^{F/F}$:Mx1 mice. Data represent two independent mice.

with other tissues such as the liver (Mizushima et al., 2004). Accordingly, significant accumulation of ubiquitinated proteins was noted in *Atg7*-deficient brain, but their levels, especially insoluble ubiquitinated proteins, were lower than in *Atg7*-deficient liver (Figures 4E and S10B), and severe formation of the inclusion was found in restricted groups of neurons (Figures 4D and S8). Moreover, unlike in the liver, detoxifying enzymes did not increase in *Atg7*-deficient brain (Figure 7A), suggesting the low susceptibility of neurons to toxicity associated with aggregate formation. In fact, several ubiquitin-positive aggregates were recognized in *Atg7*-deficient brain regions in the presence of mild neuronal loss (Komatsu et al., 2006).

Why do autophagy-deficient mice develop neurodegeneration? Analyses of Purkinje cell-specific *Atg7*-knockout mice demonstrated that *Atg7*-deficient Purkinje cells initially causes cell-autonomous, progressive dystrophy (manifested by axonal swelling) and degeneration of the axon terminals followed by cell-autonomous Purkinje cell death and mouse behavioral deficits (Komatsu et al., 2007). The mutant Purkinje cells developed aberrant organelles in the swelling axons, suggesting the important role of autophagy in the regulation of local axonal membrane trafficking and turnover, and implicate impairment of axonal autophagy as a mechanism for axonopathy associated with neurodegeneration. Importantly, such axonopathy in *Atg7*-deficient Purkinje cells and hypothalamic neurons was still observed in *Atg7*/*p62*-DKO neurons (Figures 4F, 6C, and S12), indicating that the development of axonopathy in *Atg7*-deficient neurons is *p62* independent. Therefore, we hypothesize that the mechanism of neurodegeneration caused by autophagy deficiency might involve distinct pathogenic pathways, such as axonal dystrophy and degeneration.

EXPERIMENTAL PROCEDURES

Generation of Knockout Mice

Atg7$^{F/F}$:Mx1 mice (Komatsu et al., 2005) were bred with GFP-LC3 Tg mice (Mizushima et al., 2004) to generate *Atg7*$^{F/F}$:Mx1:GFP-LC3 mice. *p62*$^{-/-}$ mice were bred with *Atg7*$^{F/F}$:Mx1, *Atg7*$^{F/F}$:Mx1:GFP-LC3, and *Atg7*$^{F/F}$:Nes mice (Komatsu et al., 2006) to generate *Atg7*$^{F/F}$:Mx1:*p62*$^{-/-}$, *Atg7*$^{F/F}$:Mx1:*p62*$^{-/-}$:GFP-LC3, and *Atg7*$^{F/F}$:Nes:*p62*$^{-/-}$ mice, respectively. With regard to deletion of *Atg7* from the liver, Cre expression in the liver was induced by intraperitoneal injection of pIpC (Sigma Chemical Co., St. Louis, MO) (Komatsu et al., 2005). Mice were housed in specific-pathogen-free facilities, and the experimental protocol was approved by the Ethics Review Committee for Animal Experimentation of Tokyo Metropolitan Institute of Medical Science. Other mice strains shown in Supplemental Data are described in Supplemental Experimental Procedures.

Immunological Analysis

Livers and brains were homogenized in 0.25 M sucrose, 10 mM 2-[4-(2-hydroxyethyl)-1-piperazinyl]ethanesulfonic acid [HEPES], pH 7.4, and 1 mM dithiothreitol (DTT). The resultant homogenates were fractionated into 0.5% Tx-100 soluble and insoluble fractions. Immunoprecipitation and immunoblot analyses were conducted as described previously (Komatsu et al., 2004). Nuclear fraction from the liver was prepared according to the method of Blobel and Potter (Blobel and Potter, 1966). The antibodies for p62, Atg7, and LC3 were described previously (Ishii et al., 1996; Komatsu et al., 2005). The antibodies for GFP (Medical and Biological Laboratories [MBL] Co., Nagoya, Japan), ubiquitin (FK2: MBL), Nrf2 (H-300: Santa Cruz Biotechnology, Inc., Santa Cruz, CA), LDH (ab2101: abcam, Inc., Cambridge, MA), actin (MAB1501R: Chemicon International, Inc., Temecula, CA) and Lamin B (M-20: Santa Cruz Biotechnology, Inc.) were purchased.

Pull-Down Assay

Recombinant GST, GST-LC3, and GST-p62 were produced in *Escherichia coli*, and recombinant proteins were purified by chromatography on glutathione-Sepharose 4B (Amersham Biosciences, Arlington Heights, IL). The GST-p62 cleaved the GST tag by precision protease (Amersham Biosciences). Purified p62 and GST or GST-LC3 were mixed in TNE buffer (Komatsu et al., 2004) for 3 hr at 4°C and then precipitated with glutathione-Sepharose. The mixtures were washed five times with ice-cold TNE. The bound proteins were analyzed by SDS-PAGE followed by Coomassie brilliant blue (CBB) staining.

Quantitative RT–PCR

cDNA was synthesized from 1 μg of total RNA using the Transcriptor First Strand cDNA Synthesis Kit (Roche Applied Science), and quantitative PCR was performed using LightCycler 480 Probes Masterin (Roche Applied Science) in a LightCycler 480 (Roche Applied Science). Signals were normalized to β-glucronidase (GUS). Primer sequences are described in Supplemental Experimental Procedures.

Immunofluorescence Microscopy of Cultured Hepatocytes

Hepatocytes grown on glass coverslips were immunostained with anti-p62 or ubiquitin (DakoCytomation, Glostrup, Denmark) antibody as described previously (Komatsu et al., 2005). The coverslips were mounted and viewed with a laser-scanning confocal microscope (FV1000, Olympus) or conventional epifluorescent microscope.

Histological Examination

Methods for tissue fixation and subsequent procedures, including H&E staining, immunohistochemistry, conventional electron microscopy, immunoelectron microscopy, and TUNEL staining were described previously (Komatsu et al., 2005, 2006). Antibodies used for immunohistochemistry and immunoelectron microscopy were as follows: rabbit polyclonal antibodies against LC3 (Komatsu et al., 2005), p62 (Ishii et al., 1996), and GFP (Abcam), and mouse monoclonal antibodies against ubiquitin (FK2 and 1B3: MBL).

Statistical Analysis

Data were analyzed by two-tailed Student's t test. For all graphs, data are represented as mean ± SD.

Supplemental Data

Supplemental Data include 13 figures, 1 table, Supplemental Experimental Procedures, and Supplemental References and can be found with this article online at http://www.cell.com/cgi/content/full/131/6/1149/DC1/.

ACKNOWLEDGMENTS

We thank T. Kaneko, T. Kouno, and K. Tatsumi for the excellent technical assistance. We also thank F. Kaji, K. Kanno, and A. Yabashi for their help in electron microscopy study and M. Kasahara for the phylogenetic tree analysis. This work was supported by grants from the

(D) The level of Nrf2 in liver nuclear fraction. Nuclear fractions were prepared from liver of the indicated genotypes at 12 days post-pIpC injection, subjected to SDS-PAGE, and analyzed by immunoblotting with antibodies against Nrf2 and Lamin B (as a control). Data represent two independent mice.

Japan Science and Technology Agency (M.K.) and the Ministry of Education, Science and Culture of Japan (M.K. and K.T.).

Received: January 5, 2007
Revised: June 26, 2007
Accepted: October 9, 2007
Published: December 13, 2007

REFERENCES

Arrasate, M., Mitra, S., Schweitzer, E.S., Segal, M.R., and Finkbeiner, S. (2004). Inclusion body formation reduces levels of mutant huntingtin and the risk of neuronal death. Nature *431*, 805–810.

Bjorkoy, G., Lamark, T., Brech, A., Outzen, H., Perander, M., Overvatn, A., Stenmark, H., and Johansen, T. (2005). p62/SQSTM1 forms protein aggregates degraded by autophagy and has a protective effect on huntingtin-induced cell death. J. Cell Biol. *171*, 603–614.

Blobel, G., and Potter, V.R. (1966). Nuclei from rat liver: isolation method that combines purity with high yield. Science *154*, 1662–1665.

Elmore, S.P., Qian, T., Grissom, S.F., and Lemasters, J.J. (2001). The mitochondrial permeability transition initiates autophagy in rat hepatocytes. FASEB J. *15*, 2286–2287.

Fortun, J., Dunn, W.A., Jr., Joy, S., Li, J., and Notterpek, L. (2003). Emerging role for autophagy in the removal of aggresomes in Schwann cells. J. Neurosci. *23*, 10672–10680.

Goldberg, A.L. (2003). Protein degradation and protection against misfolded or damaged proteins. Nature *426*, 895–899.

Hara, T., Nakamura, K., Matsui, M., Yamamoto, A., Nakahara, Y., Suzuki-Migishima, R., Yokoyama, M., Mishima, K., Saito, I., Okano, H., and Mizushima, N. (2006). Suppression of basal autophagy in neural cells causes neurodegenerative disease in mice. Nature *441*, 885–889.

Ichimura, Y., Kirisako, T., Takao, T., Satomi, Y., Shimonishi, Y., Ishihara, N., Mizushima, N., Tanida, I., Kominami, E., Ohsumi, M., et al. (2000). A ubiquitin-like system mediates protein lipidation. Nature *408*, 488–492.

Ishii, T., Yanagawa, T., Kawane, T., Yuki, K., Seita, J., Yoshida, H., and Bannai, S. (1996). Murine peritoneal macrophages induce a novel 60-kDa protein with structural similarity to a tyrosine kinase p56lck-associated protein in response to oxidative stress. Biochem. Biophys. Res. Commun. *226*, 456–460.

Iwata, J., Ezaki, J., Komatsu, M., Yokota, S., Ueno, T., Tanida, I., Chiba, T., Tanaka, K., and Kominami, E. (2006). Excess peroxisomes are degraded by autophagic machinery in mammals. J. Biol. Chem. *281*, 4035–4041.

Kabeya, Y., Mizushima, N., Ueno, T., Yamamoto, A., Kirisako, T., Noda, T., Kominami, E., Ohsumi, Y., and Yoshimori, T. (2000). LC3, a mammalian homologue of yeast Apg8p, is localized in autophagosome membranes after processing. EMBO J. *19*, 5720–5728.

Kamimoto, T., Shoji, S., Hidvegi, T., Mizushima, N., Umebayashi, K., Perlmutter, D.H., and Yoshimori, T. (2006). Intracellular inclusions containing mutant alpha1-antitrypsin Z are propagated in the absence of autophagic activity. J. Biol. Chem. *281*, 4467–4476.

Komatsu, M., Chiba, T., Tatsumi, K., Iemura, S., Tanida, I., Okazaki, N., Ueno, T., Kominami, E., Natsume, T., and Tanaka, K. (2004). A novel protein-conjugating system for Ufm1, a ubiquitin-fold modifier. EMBO J. *23*, 1977–1986.

Komatsu, M., Waguri, S., Ueno, T., Iwata, J., Murata, S., Tanida, I., Ezaki, J., Mizushima, N., Ohsumi, Y., Uchiyama, Y., et al. (2005). Impairment of starvation-induced and constitutive autophagy in Atg7-deficient mice. J. Cell Biol. *169*, 425–434.

Komatsu, M., Waguri, S., Chiba, T., Murata, S., Iwata, J., Tanida, I., Ueno, T., Koike, M., Uchiyama, Y., Kominami, E., and Tanaka, K. (2006). Loss of autophagy in the central nervous system causes neurodegeneration in mice. Nature *441*, 880–884.

Komatsu, M., Wang, Q.J., Holstein, G.R., Friedrich, V.L., Iwata, J.I., Kominami, E., Chait, B.T., Tanaka, K., and Yue, Z. (2007). Essential role for autophagy protein Atg7 in the maintenance of axonal homeostasis and the prevention of axonal degeneration. Proc. Natl. Acad. Sci. USA *104*, 14489–14494.

Kuma, A., Hatano, M., Matsui, M., Yamamoto, A., Nakaya, H., Yoshimori, T., Ohsumi, Y., Tokuhisa, T., and Mizushima, N. (2004). The role of autophagy during the early neonatal starvation period. Nature *432*, 1032–1036.

Kuusisto, E., Salminen, A., and Alafuzoff, I. (2001). Ubiquitin-binding protein p62 is present in neuronal and glial inclusions in human tauopathies and synucleinopathies. Neuroreport *12*, 2085–2090.

Lamark, T., Perander, M., Outzen, H., Kristiansen, K., Overvatn, A., Michaelsen, E., Bjorkoy, G., and Johansen, T. (2003). Interaction codes within the family of mammalian Phox and Bem1p domain-containing proteins. J. Biol. Chem. *278*, 34568–34581.

Levine, B., and Klionsky, D.J. (2004). Development by self-digestion: molecular mechanisms and biological functions of autophagy. Dev. Cell *6*, 463–477.

Mizushima, N., Yamamoto, A., Hatano, M., Kobayashi, Y., Kabeya, Y., Suzuki, K., Tokuhisa, T., Ohsumi, Y., and Yoshimori, T. (2001). Dissection of autophagosome formation using Apg5-deficient mouse embryonic stem cells. J. Cell Biol. *152*, 657–668.

Mizushima, N., Yamamoto, A., Matsui, M., Yoshimori, T., and Ohsumi, Y. (2004). In vivo analysis of autophagy in response to nutrient starvation using transgenic mice expressing a fluorescent autophagosome marker. Mol. Biol. Cell *15*, 1101–1111.

Moscat, J., Diaz-Meco, M.T., Albert, A., and Campuzano, S. (2006). Cell signaling and function organized by PB1 domain interactions. Mol. Cell *23*, 631–640.

Nakano, T., Nakaso, K., Nakashima, K., and Ohama, E. (2004). Expression of ubiquitin-binding protein p62 in ubiquitin-immunoreactive intraneuronal inclusions in amyotrophic lateral sclerosis with dementia: analysis of five autopsy cases with broad clinicopathological spectrum. Acta Neuropathol. (Berl.) *107*, 359–364.

Ohsumi, Y. (2001). Molecular dissection of autophagy: two ubiquitin-like systems. Nat. Rev. Mol. Cell Biol. *2*, 211–216.

Ravikumar, B., Vacher, C., Berger, Z., Davies, J.E., Luo, S., Oroz, L.G., Scaravilli, F., Easton, D.F., Duden, R., O'Kane, C.J., and Rubinsztein, D.C. (2004). Inhibition of mTOR induces autophagy and reduces toxicity of polyglutamine expansions in fly and mouse models of Huntington disease. Nat. Genet. *36*, 585–595.

Rodriguez, A., Duran, A., Selloum, M., Champy, M.F., Diez-Guerra, F.J., Flores, J.M., Serrano, M., Auwerx, J., Diaz-Meco, M.T., and Moscat, J. (2006). Mature-onset obesity and insulin resistance in mice deficient in the signaling adapter p62. Cell Metab. *3*, 211–222.

Ross, C.A., and Poirier, M.A. (2005). Opinion: What is the role of protein aggregation in neurodegeneration? Nat. Rev. Mol. Cell Biol. *6*, 891–898.

Sanchez, P., De Carcer, G., Sandoval, I.V., Moscat, J., and Diaz-Meco, M.T. (1998). Localization of atypical protein kinase C isoforms into lysosome-targeted endosomes through interaction with p62. Mol. Cell. Biol. *18*, 3069–3080.

Sanchez, I., Mahlke, C., and Yuan, J. (2003). Pivotal role of oligomerization in expanded polyglutamine neurodegenerative disorders. Nature *421*, 373–379.

Stumptner, C., Fuchsbichler, A., Heid, H., Zatloukal, K., and Denk, H. (2002). Mallory body–a disease-associated type of sequestosome. Hepatology *35*, 1053–1062.

Tabner, B.J., El-Agnaf, O.M., German, M.J., Fullwood, N.J., and Allsop, D. (2005). Protein aggregation, metals and oxidative stress in neurodegenerative diseases. Biochem. Soc. Trans. *33*, 1082–1086.

Tong, K.I., Kobayashi, A., Katsuoka, F., and Yamamoto, M. (2006). Two-site substrate recognition model for the Keap1-Nrf2 system: a hinge and latch mechanism. Biol. Chem. *387*, 1311–1320.

Tsukada, M., and Ohsumi, Y. (1993). Isolation and characterization of autophagy-defective mutants of Saccharomyces cerevisiae. FEBS Lett. *333*, 169–174.

Wang, Q.J., Ding, Y., Kohtz, D.S., Mizushima, N., Cristea, I.M., Rout, M.P., Chait, B.T., Zhong, Y., Heintz, N., and Yue, Z. (2006). Induction of autophagy in axonal dystrophy and degeneration. J. Neurosci. *26*, 8057–8068.

Wooten, M.W., Hu, X., Babu, J.R., Seibenhener, M.L., Geetha, T., Paine, M.G., and Wooten, M.C. (2006). Signaling, polyubiquitination, trafficking, and inclusions: Sequestosome 1/p62's role in neurodegenerative disease. J. Biomed. Biotechnol. *2006*, 62079.

doi:10.1038/nature04723

LETTERS

Loss of autophagy in the central nervous system causes neurodegeneration in mice

Masaaki Komatsu[1,2]*, Satoshi Waguri[3]*†, Tomoki Chiba[1], Shigeo Murata[1], Jun-ichi Iwata[1,2], Isei Tanida[2], Takashi Ueno[2], Masato Koike[3], Yasuo Uchiyama[3], Eiki Kominami[2] & Keiji Tanaka[1]

Protein quality-control, especially the removal of proteins with aberrant structures, has an important role in maintaining the homeostasis of non-dividing neural cells[1]. In addition to the ubiquitin–proteasome system, emerging evidence points to the importance of autophagy—the bulk protein degradation pathway involved in starvation-induced and constitutive protein turnover—in the protein quality-control process[2,3]. However, little is known about the precise roles of autophagy in neurons. Here we report that loss of *Atg7* (autophagy-related 7), a gene essential for autophagy, leads to neurodegeneration. We found that mice lacking *Atg7* specifically in the central nervous system showed behavioural defects, including abnormal limb-clasping reflexes and a reduction in coordinated movement, and died within 28 weeks of birth. *Atg7* deficiency caused massive neuronal loss in the cerebral and cerebellar cortices. Notably, polyubiquitinated proteins accumulated in autophagy-deficient neurons as inclusion bodies, which increased in size and number with ageing. There was, however, no obvious alteration in proteasome function. Our results indicate that autophagy is essential for the survival of neural cells, and that impairment of autophagy is implicated in the pathogenesis of neurodegenerative disorders involving ubiquitin-containing inclusion bodies.

Macroautophagy (hereafter referred to as autophagy) is an evolutionarily conserved pathway in which the cytoplasm and organelles are engulfed within double-membraned vesicles, known as autophagosomes, in preparation for the turnover and recycling of these cellular constituents[4]. Genetic studies using various model organisms have highlighted the importance of autophagy in physiological and pathological events[5]. The principal role of autophagy is in the supply of nutrients for survival, as shown in yeast[6] and early neonatal mice[7,8]. Autophagy also has a role in cellular remodelling during differentiation and the development of multicellular organisms, such as dauer formation in *Caenorhabditis elegans*[9] and metamorphosis in *Drosophila melanogaster*[10]. Moreover, constitutive autophagy, which occurs independently of nutrient stress, contributes to mouse liver homeostasis[8], major histocompatibility class (MHC) II antigen presentation[11], and cellular defence against invading streptococci[12] and *Mycobacterium tuberculosis*[13]. However, the physiological functions of autophagy, particularly in neurons, are still largely unknown.

To examine the relationship between neuronal pathology and autophagy deficiency *in vivo*, we crossed *Atg7*-conditional knockout mice ($Atg7^{flox/flox}$) (ref. 8) with transgenic mice expressing Cre recombinase under the control of the nestin promoter (nestin-*Cre*) (ref. 14), to produce mice deficient for *Atg7* specifically in the central nervous system ($Atg7^{flox/flox}$; nestin-*Cre*). Atg7 is an E1-like enzyme for both the Atg12- and Atg8-conjugation systems[15], and is essential

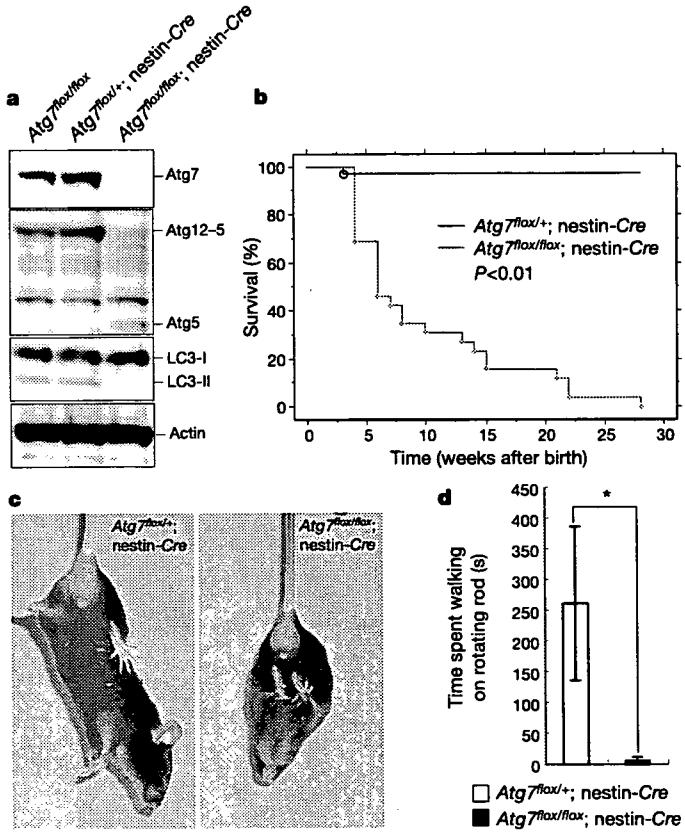

Figure 1 | Behavioural disorder in $Atg7^{flox/flox}$; nestin-Cre mice. **a**, Impairment of two ATG-conjugation systems (Atg12 and LC3) in the Atg7-deficient brain. Brain homogenates from P28 mice were immunoblotted with antibodies against Atg7, Atg5 and LC3. Actin was used as a loading control. Data shown are representative of three separate experiments. **b**, Kaplan–Meier survival curves of $Atg7^{flox/+}$; nestin-*Cre* ($n = 41$) and $Atg7^{flox/flox}$; nestin-*Cre* ($n = 26$) mice over 28 weeks. **c**, Abnormal limb-clasping reflexes in $Atg7^{flox/flox}$; nestin-*Cre* mice at P28. When lifted by the tail, $Atg7^{flox/+}$; nestin-*Cre* mice behave normally, extending their hind limbs and bodies. In contrast, $Atg7^{flox/flox}$; nestin-*Cre* mice bend their legs towards their trunk or tighten their back limbs to their bodies and anterior limbs. **d**, Movement ataxia in $Atg7^{flox/flox}$; nestin-*Cre* mice at P28. Motor coordination was tested using a rotarod assay. $Atg7^{flox/+}$; nestin-*Cre* ($n = 5$) and $Atg7^{flox/flox}$; nestin-*Cre* ($n = 5$) mice were placed on a rod rotating at 20 r.p.m., and the time spent on the rod was counted. Data show mean ± s.d. *, $P < 0.01$ (Student's *t*-test). There was no significant sex difference in survival rate and onset-stage of abnormal limb-clasping and tremor in $Atg7^{flox/flox}$; nestin-*Cre* mice.

[1]Laboratory of Frontier Science, Tokyo Metropolitan Institute of Medical Science, Bunkyo-ku, Tokyo 113-8613, Japan. [2]Department of Biochemistry, Juntendo University School of Medicine, Bunkyo-ku, Tokyo 113-8421, Japan. [3]Department of Cell Biology and Neurosciences, Osaka University Graduate School of Medicine, Osaka 565-0871, Japan. †Present address: Department of Anatomy and Histology, Fukushima Medical University School of Medicine, 1 Hikarigaoka, Fukushima 960-1295, Japan.
*These authors contributed equally to this work.

for autophagy[8]. Atg7 protein was absent at postnatal day (P)28 in brain from *Atg7*$^{flox/flox}$; nestin-*Cre* but not control (*Atg7*$^{flox/+}$; nestin-*Cre*) mice (Fig. 1a). The level of Atg7 protein in other tissues such as liver, lung, heart and muscle was comparable between *Atg7*$^{flox/flox}$; nestin-*Cre* and control mice (data not shown). Atg12–Atg5 conjugate was detected only in the brains of control mice by immunoblotting with an anti-Atg5 antibody (Fig. 1a). In contrast, free Atg5, which was faintly observed in the control mouse brain, was clearly increased in the mutant brain (Fig. 1a). The mammalian homologue of yeast Atg8, microtubule-associated protein 1 light-chain 3 (LC3), exists in two forms (LC3-I and LC3-II)[16]. Both forms were detected in brains from control mice, but only the LC3-I form was detected in *Atg7*$^{flox/flox}$; nestin-*Cre* brain (Fig. 1a). The loss of both Atg7 and LC3-II proteins was observed from P0 in the brain of *Atg7*$^{flox/flox}$; nestin-*Cre* mice (Supplementary Fig. S1). These results indicate complete impairment of autophagy in the central nervous system of *Atg7*$^{flox/flox}$; nestin-*Cre* mice after birth.

Atg7$^{flox/flox}$; nestin-*Cre* mice were viable at birth and indistinguishable in appearance from their littermates. However, the survival rate of the mutant mice diminished markedly by four weeks after birth, and all *Atg7*$^{flox/flox}$; nestin-*Cre* mice were dead within 28 weeks (Fig. 1b). We also observed growth retardation as early as P14 in these mice (data not shown). Furthermore, the mice showed motor and behavioural deficits, including abnormal limb-clasping reflexes (Fig. 1c) and tremor, and in some cases, they walked on their tiptoes. In a rotarod test, most *Atg7*$^{flox/flox}$; nestin-*Cre* mice fell after grasping the rod only briefly (Fig. 1d). These motor and behavioural deficits began to appear at P14–P21. These results suggest that autophagy deficiency in the central nervous system results in a severe neurological disorder.

Histological analysis using Meyer's haematoxylin and eosin (H&E) staining showed marked atrophy of the cerebral cortical region of *Atg7*$^{flox/flox}$; nestin-*Cre* brain at P56 (Fig. 2a, b). The ratios of cortical thickness to dorsoventral thickness of the brain in *Atg7*$^{flox/+}$; nestin-*Cre* and *Atg7*$^{flox/flox}$; nestin-*Cre* mice were 0.17 ± 0.00031 and 0.15 ± 0.00034, respectively ($n = 5$, $P < 0.01$). Notably, almost no large pyramidal neurons were observed in *Atg7*$^{flox/flox}$; nestin-*Cre* mice compared with the corresponding region in brains from control mice (Fig. 2c, d). Immunostaining for the glial marker GFAP (glial fibrillary acidic protein) showed an increase in GFAP signal in the cerebral cortex of *Atg7*$^{flox/flox}$; nestin-*Cre* mice (Fig. 2e, f), suggesting the presence of neuronal damage in this region. In the cerebellar

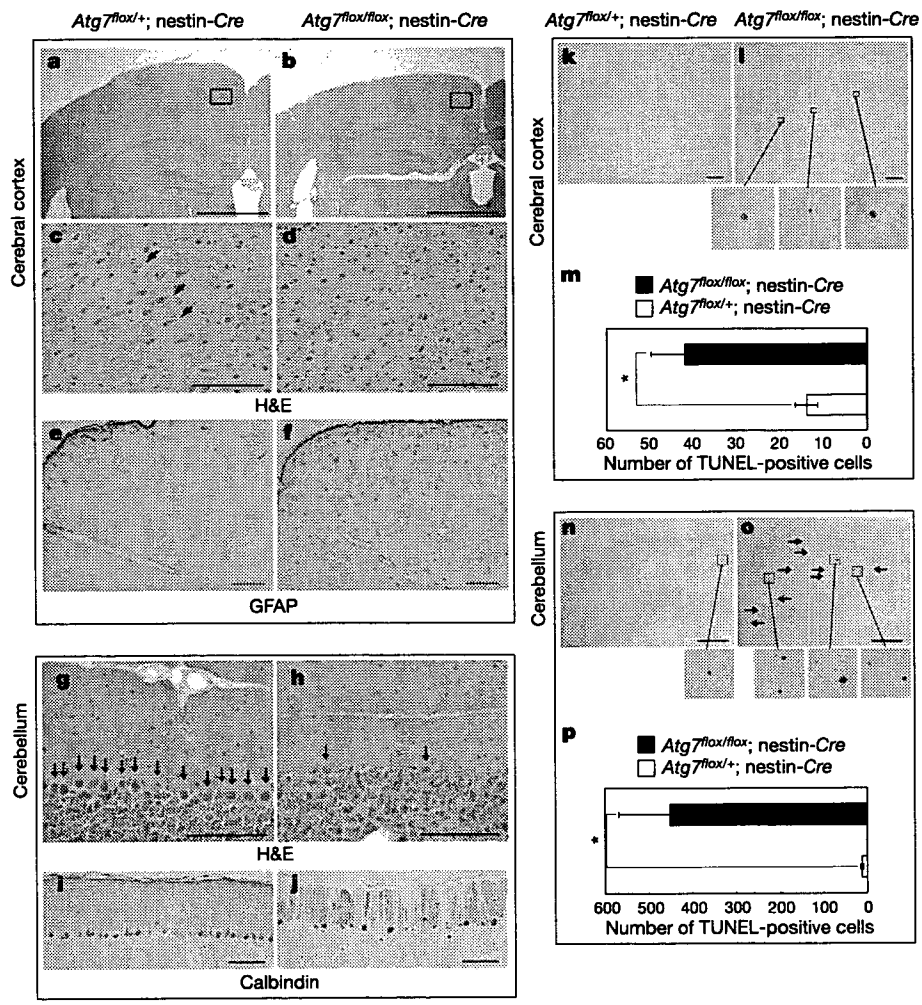

Figure 2 | Marked cell death in autophagy-deficient cerebral cortex and cerebellum. a–f, Histological analyses of *Atg7*$^{flox/+}$; nestin-*Cre* (left) and *Atg7*$^{flox/flox}$; nestin-*Cre* (right) cerebral cortex at P56. Cryosections were stained with H&E (**a–d**) or immunostained for the glial marker GFAP (**e**, **f**). Boxed areas in **a** and **b** are magnified in **c** and **d**, respectively. Arrows in **c** point to large pyramidal neurons in the cerebral cortex. **g–j**, Histological analysis of *Atg7*$^{flox/+}$; nestin-*Cre* (left) and *Atg7*$^{flox/flox}$; nestin-*Cre* (right) cerebellum at P56. Cryosections were stained with H&E (**g**, **h**) or immunostained for the Purkinje marker calbindin (**i**, **j**). Arrows in **g** and **h** indicate cerebellar Purkinje cells. **k–p**, TUNEL staining of the cerebral cortex (**k**, **l**) and cerebellum (**n**, **o**) at P56 in *Atg7*$^{flox/+}$; nestin-*Cre* (**k**, **n**) and *Atg7*$^{flox/flox}$; nestin-*Cre* (**l**, **o**) sections. TUNEL-positive cells are indicated with arrows and shown as higher magnification images beneath panels **l**, **n** and **o**. Histograms show the average number (±s.d.) of TUNEL-positive cells in ten sections for three animals of each genotype (**m**, **p**). *, $P < 0.05$ (*t*-test). Scale bars, 1 mm (**a**, **b**), 100 μm (**c–j**), 250 μm (**k**, **l**, **n**, **o**). We observed no sex difference in brain morphology or neuronal loss in *Atg7*$^{flox/flox}$; nestin-*Cre* mice.

cortex, H&E staining revealed a large reduction in the number of Purkinje cells in the mutant brain (Fig. 2g, h), which was further confirmed by immunolabelling of Purkinje cells with an anti-calbindin antibody (Fig. 2i, j). Similar neuronal loss was also recognized in the hippocampal pyramidal cell layer of mutant brain (Supplementary Fig. S2).

To determine whether the reduced number of neurons observed in *Atg7*$^{flox/flox}$; nestin-*Cre* mouse brain was caused by cell death, we performed TUNEL (TdT-mediated dUTP nick end labelling) assays. We observed a marked increase in the number of TUNEL-positive cells in the cerebral cortex (Fig. 2k–m) and granular cell layer of the cerebellum at P56 in *Atg7*$^{flox/flox}$; nestin-*Cre* mice (Fig. 2n–p) compared with control mouse brains. Although loss of Purkinje cells was observed in the mutant brain, we could not detect TUNEL-positive Purkinje cells at any developmental stage examined. However, when *Atg7* was specifically depleted in Purkinje cells using transgenic mice expressing Cre recombinase under the control of the *Pcp2* gene promoter (Pcp2-*Cre*), a marked reduction in the number of Purkinje cells was detected in the absence of TUNEL reactivity (data not shown), suggesting that neurons deficient in autophagy can die in a cell-autonomous fashion. Together, these results indicate that lack of autophagy in the central nervous system leads to neurodegeneration.

We have previously reported that autophagy is responsible for constitutive protein turnover in quiescent hepatocytes even under nutrient-rich conditions, and that a defect in autophagy leads to the accumulation of large, ubiquitin-containing inclusion bodies[8]. We therefore probed brain sections with an anti-ubiquitin antibody to examine the presence of ubiquitin-containing inclusion bodies. At P56, ubiquitin-positive dots were detected in several regions of the *Atg7*$^{flox/flox}$; nestin-*Cre* mouse brain, including the cerebral cortex (Fig. 3b), cerebellar Purkinje cells (Fig. 3d), hippocampal pyramidal neurons (Fig. 3f), thalamus (data not shown), hypothalamus (Fig. 3h), amygdala (Fig. 3j) and pontine nuclei (Fig. 3l). The degree of staining varied by region. For example, whereas most neuronal

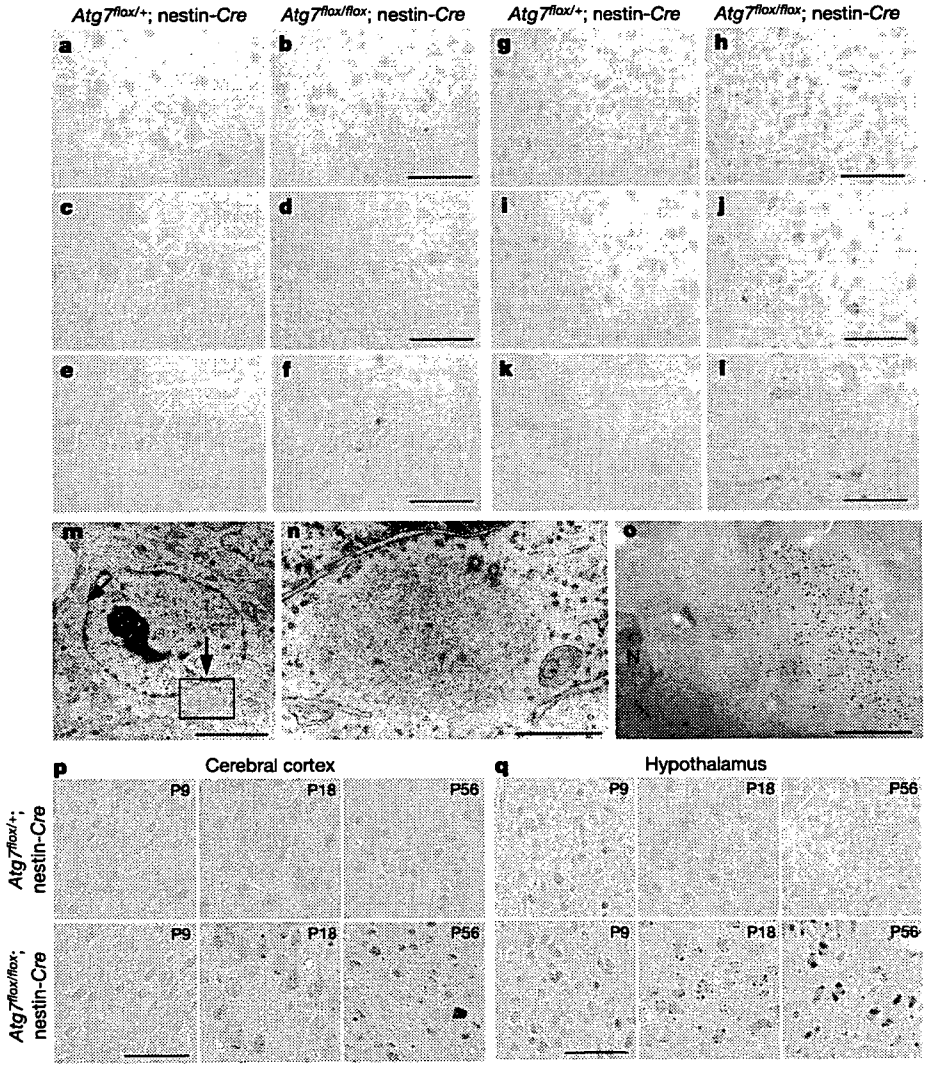

Figure 3 | Appearance of ubiquitin-positive inclusions in autophagy-deficient neurons. a–l, The presence of ubiquitin-positive dots was examined immunohistochemically in several regions including cerebral cortex (**a**, **b**), cerebellum (**c**, **d**), hippocampus (**e**, **f**), hypothalamus (**g**, **h**), amygdala (**i**, **j**) and pontine nuclei (**k**, **l**) of *Atg7*$^{flox/+}$; nestin-*Cre* and *Atg7*$^{flox/flox}$; nestin-*Cre* mice. Note the presence of numerous ubiquitin dots in the amygdala and hypothalamus of the representative mutants. Scale bars, 50 μm. **m**, **n**, Electron micrographs of the brain of *Atg7*$^{flox/flox}$; nestin-*Cre* mice. Inclusion bodies (arrows) were often observed in *Atg7*$^{flox/flox}$; nestin-*Cre* hypothalamus. The boxed region in **m** is shown in **n**. Inclusion bodies were not detected in *Atg7*$^{flox/+}$; nestin-*Cre* brain (data not shown). Scale bars, 5 μm (**m**), 1 μm (**n**). **o**, Immunoelectron micrograph of ubiquitin in a representative *Atg7*$^{flox/flox}$; nestin-*Cre* hypothalamus. N, nucleus. Scale bar, 1 μm. **p**, **q**, Immunohistochemical detection of ubiquitin-positive inclusions in the cerebral cortex (**p**) and hypothalamus (**q**) at P9, P18 and P56. Brain sections of each genotype at the indicated ages were immunostained with an anti-ubiquitin antibody. Ubiquitin-positive inclusions appeared at P18 and became larger with ageing in the brain of *Atg7*$^{flox/flox}$; nestin-*Cre* mice. Scale bars, 50 μm.

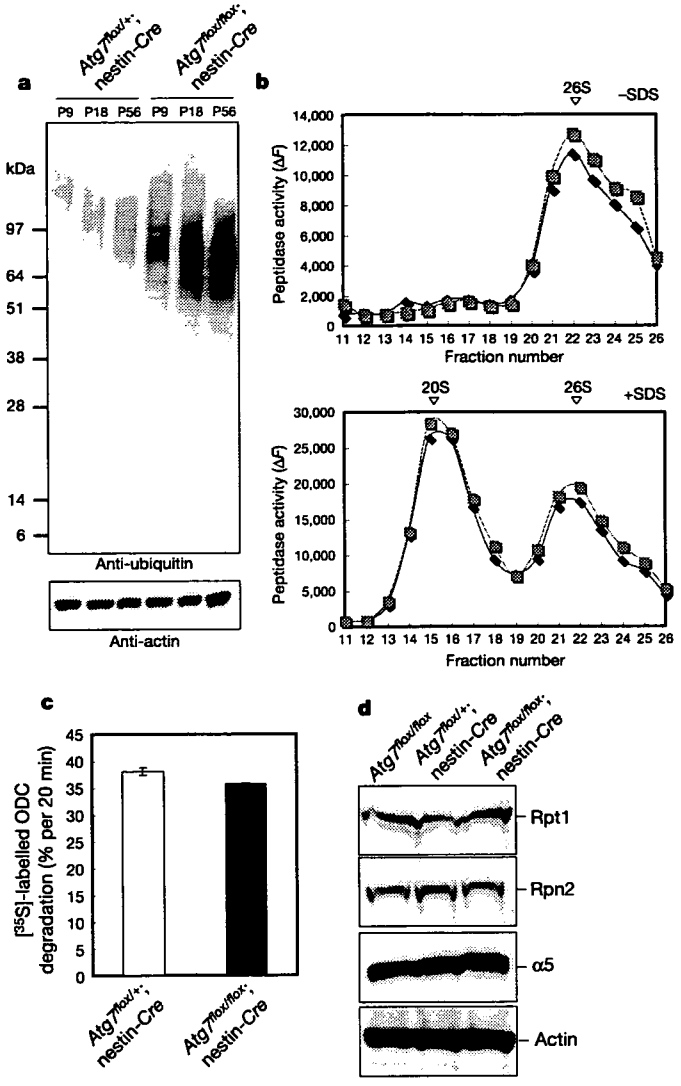

Figure 4 | Qualitative and quantitative analyses of proteasomes in autophagy-deficient brain. a, Increase in ubiquitinated proteins in *Atg7*$^{flox/flox}$; nestin-*Cre* mouse brain over time. Homogenates of P9, P18 and P56 brains from *Atg7*$^{flox/+}$; nestin-*Cre* and *Atg7*$^{flox/flox}$; nestin-*Cre* mice were immunoblotted with an anti-ubiquitin antibody. An anti-actin antibody was used as a loading control. Data shown are representative of three separate experiments. We observed no sex difference in the accumulation of ubiquitin in *Atg7*$^{flox/flox}$; nestin-*Cre* mice. **b**, Peptide hydrolysis activity of 20S and 26S proteasomes. Homogenates from P28 *Atg7*$^{flox/+}$; nestin-*Cre* (blue) and *Atg7*$^{flox/flox}$; nestin-*Cre* (pink) brains were fractionated by glycerol density gradient centrifugation (10–40% glycerol from fraction 1 to fraction 30). Aliquots from each fraction were used for the assay of chymotryptic activity of proteasomes using Suc-LLVY-AMC as a substrate in the absence (top) or presence (bottom) of 0.05% SDS. The sedimenting positions of 20S and 26S proteasomes are indicated with arrowheads. Note that whereas 26S proteasomes exist in active forms in tissues, 20S proteasomes are latent and are activated artificially by a low concentration of SDS. **c**, ATP-dependent degradation of [^{35}S]-labelled ODC. Degradation of [^{35}S]-labelled ODC was assayed using crude extracts from P28 *Atg7*$^{flox/+}$; nestin-*Cre* and *Atg7*$^{flox/flox}$; nestin-*Cre* brains. The experiment was repeated three times, and values represent mean ± s.d. In the above assays, there were no significant differences between *Atg7*$^{flox/+}$; nestin-*Cre* and *Atg7*$^{flox/flox}$; nestin-*Cre* mice. **d**, Immunoblot analysis of 26S proteasome components. Homogenates from P28 *Atg7*$^{flox/flox}$, *Atg7*$^{flox/+}$; nestin-*Cre* and *Atg7*$^{flox/flox}$; nestin-*Cre* brains were immunoblotted with antibodies against the indicated proteins. Data shown are representative of three separate experiments. There was no change in proteasome status for the different genotypes.

cells in the amygdala (Fig. 3j) and hypothalamus (Fig. 3h) contained several ubiquitin dots of small to large size, only a small number of cerebellar Purkinje cells stained for ubiquitin, and the immunoreactive dots were of small size (Fig. 3d). Electron microscopy showed that *Atg7*$^{flox/flox}$; nestin-*Cre* hypothalamic neurons had circular or elliptical large structures composed of fibrillar elements in the perikarya (Fig. 3m, n). Immunoelectron microscopy further confirmed that these aberrant structures contained ubiquitin (Fig. 3o). These ubiquitin dots appeared not only in the perikarya of neurons, but also in the intercellular space (see Fig. 3h, j, l). Dots found in the intercellular space might correspond to ubiquitin inside neurites, because they were observed in myelinated axons around pontine nuclei using both light and electron microscopy (Supplementary Fig. S3a, b). In contrast, almost no ubiquitin dots were observed in astroglial cells (Supplementary Fig. S3c). Together with the results in Fig. 3, we concluded that most of the distinct ubiquitin dots were located in neurons.

We examined the development of ubiquitin-containing inclusion bodies at different stages by dissecting the brains of *Atg7*$^{flox/+}$; nestin-*Cre* and *Atg7*$^{flox/flox}$; nestin-*Cre* mice at P9, P18 and P56. Only a few ubiquitin-positive aggregates were noted in the neurons of control and mutant cerebral cortex and hypothalamus at P9 (Fig. 3p, q). In contrast, several ubiquitin-containing inclusions were clearly noted in *Atg7*$^{flox/flox}$; nestin-*Cre* cortex and hypothalamus at P18, increasing in number and size by P56 (Fig. 3p, q). These results indicate an age-dependent increase in ubiquitin-containing inclusion bodies in autophagy-deficient neurons. Consistent with the above immunohistochemical analysis (Fig. 3p, q), immunoblot analysis revealed increasing levels of high-molecular-mass polyubiquitinated proteins with age in the brains of *Atg7*$^{flox/flox}$; nestin-*Cre* mice (Fig. 4a), and an increase in their insoluble forms at later developmental stages (data not shown).

Finally, we examined whether autophagy deficiency influences proteasome functions. The chymotryptic activities of 26S and 20S proteasomes (measured using Suc-LLVY-MCA as a substrate) were comparable in extracts from both control and *Atg7*$^{flox/flox}$; nestin-*Cre* brains (Fig. 4b). Furthermore, the ATP-dependent degradation of ornithine decarboxylase (ODC) by 26S proteasomes was similar in control and mutant brains (Fig. 4c). Moreover, the relative amounts of several subunits of the 26S proteasome did not change in the brain irrespective of autophagy deficiency (as detected by immunoblotting, Fig. 4d). These results indicate that age-dependent accumulation of ubiquitin-positive aggregates in the autophagy-deficient brain occurs despite the apparently normal function of proteasomes.

Over the past decade, researchers working in the field of neurodegenerative diseases have made great progress in uncovering the mechanisms of these disorders by focusing on the interplay between proteolytic stress and neural cell death[17,18]. Increasing evidence indicates that ubiquitin-positive inclusion bodies—the pathological hallmark of various neurodegenerative diseases—are formed by dysfunction of proteasome degrading machinery[3]. Indeed, proteins with aberrant structure impair proteasome functions directly, thus attenuating 'garbage disposal'[19]. On the other hand, the accumulation of autophagosomes owing to impairment of fusion with lysosomes is observed in various disorders, including Alzheimer's disease[20–22], and it has been proposed that autophagy functions to degrade toxic proteins in familial neurodegenerative diseases[23–25]. However, it remains unknown whether these two proteolytic systems work independently or cooperatively to maintain protein homeostasis in cells. Furthermore, whether autophagy has a role in cell death or cell survival is currently under debate[26].

We have shown that *Atg7*$^{flox/flox}$; nestin-*Cre* mice exhibit neurological abnormalities and neuronal death, suggesting that impaired autophagy causes neurodegeneration. We suggest a particularly important role for autophagy in the brain, to which nutrients must be constantly supplied from other organs, even under fasting conditions. Moreover, we find that autophagy deficiency in neurons leads to the accumulation of ubiquitin-containing inclusion bodies,

without obvious deficits in proteasome function. Hence, our data indicate a central role for constitutive autophagy in the elimination of unfavourable proteins and in the survival of neurons, independent of the proteasome system (see the proposed model in Supplementary Fig. S4). Although we do not know whether autophagy and proteasome degradation target a similar set of normal and/or misfolded proteins, it is plausible that the autophagic pathway assists in degrading accumulated intractable proteins when cellular levels of aberrant proteins overwhelm the disposal capacity of the proteasome.

We have shown that a lack of autophagy is associated with neurodegeneration, even in the absence of harmful gene products found in neurodegenerative disorders such as Huntington's disease, Parkinson's disease and amyotrophic lateral sclerosis. We therefore predict that the role of autophagy becomes even more critical in the pathogenesis of such neurodegenerative diseases, when disease-related, aggregation-prone proteins are expressed as a result of genetic mutations and/or environmental insults, leading to early-onset symptoms.

METHODS

Animals. Nestin-*Cre* transgenic mice[14] were purchased from the Jackson Laboratory. *Atg7*$^{flox/flox}$ mice[8] were bred with nestin-*Cre* transgenic mice to produce *Atg7*$^{flox/flox}$; nestin-*Cre* mice. Mice were housed in a pathogen-free facility. Motor function was assessed using a rotarod test[27]. Experimental protocols were approved by the Ethics Review Committee for Animal Experimentation at the Tokyo Metropolitan Institute of Medical Science.

Immunoblot analysis. Immunoblots were carried out as described previously[8]. Antibodies against Atg7, Atg5 and LC3 have been described previously[8]. Antibodies against Rpt1, Rpn2 and α5 were provided by K. B. Hendil. Polyclonal anti-ubiquitin (FK2; Medical & Biological Laboratories) and anti-actin (MAB1501R; Chemicon) antibodies were also used.

Histological examination. *Atg7*$^{flox/+}$; nestin-*Cre* and *Atg7*$^{flox/flox}$; nestin-*Cre* mice were fixed by cardiac perfusion with 0.1 M phosphate buffer containing 4% paraformaldehyde, 4% sucrose for light microscopy and immunohistochemistry, with 0.1 M phosphate buffer containing 2% paraformaldehyde, 2% glutaraldehyde for standard electron microscopy, or with 0.1 M phosphate buffer containing 4% paraformaldehyde, 0.1% glutaraldehyde for immunoelectron microscopy. Brain tissues were excised and processed for morphological analysis as described previously[8,28]. For light microscopic analysis, 10-μm cryosections were cut and stained with H&E or immunolabelled with the following antibodies: anti-human NeuN (Abcam), anti-GFAP (Sigma), anti-calbindin (Sigma), anti-myelin basic protein (MBP; MCA409S, Serotec) and anti-ubiquitin (DAKO) antibodies. The TUNEL assay has been described previously[28]. For counting TUNEL-positive signals in the cerebral cortex, 60 coronal sections containing the anterior portion of the hippocampus (~0.6-mm thick in total) were cut, and TUNEL staining was performed on every sixth section, on a total of ten sections.

Electron microscopy and immunoelectron microscopy. Fixed brains were post-fixed with 1% OsO_4, embedded in Epon812 and sectioned. Immunoelectron microscopy was carried out on cryothin sections as described previously[29]. In brief, brains were frozen in phosphate buffer containing 2.3 M sucrose and 20% polyvinyl pyrrhoridon. Ultrathin sections were mounted on Formvar carbon-coated nickel grids, blocked with 1% bovine serum albumin (BSA) in PBS, and incubated with anti-ubiquitin antibody (1B3) and colloidal gold-conjugated secondary antibody.

Glycerol gradient analysis. Samples were fractionated by 10–40% (v/v) linear glycerol density gradient centrifugation (22 h, 100,000*g*) as described previously[30].

Assay of proteasome activity. Peptidase activity was measured using a fluorescent peptide substrate, succinyl-Leu-Leu-Val-Tyr-7-amido-4-methylcoumarin (Suc-LLVY-MCA), as described previously[30]. Ornithine decarboxylase (ODC)-degradation activity was assayed as described previously[30].

Received 6 February; accepted 20 March 2006.
Published online 19 April 2006.

1. Forman, M. S., Trojanowski, J. Q. & Lee, V. M. Neurodegenerative diseases: a decade of discoveries paves the way for therapeutic breakthroughs. *Nature Med.* **10**, 1055–1063 (2004).
2. Shintani, T. & Klionsky, D. J. Autophagy in health and disease: a double-edged sword. *Science* **306**, 990–995 (2004).
3. Goldberg, A. L. Protein degradation and protection against misfolded or damaged proteins. *Nature* **426**, 895–899 (2003).
4. Reggiori, F. & Klionsky, D. J. Autophagosomes: biogenesis from scratch? *Curr. Opin. Cell Biol.* **17**, 415–422 (2005).
5. Levine, B. & Klionsky, D. J. Development by self-digestion: molecular mechanisms and biological functions of autophagy. *Dev. Cell* **6**, 463–477 (2004).
6. Tsukada, M. & Ohsumi, Y. Isolation and characterization of autophagy-defective mutants of *Saccharomyces cerevisiae*. *FEBS Lett.* **333**, 169–174 (1993).
7. Kuma, A. *et al.* The role of autophagy during the early neonatal starvation period. *Nature* **432**, 1032–1036 (2004).
8. Komatsu, M. *et al.* Impairment of starvation-induced and constitutive autophagy in *Atg7*-deficient mice. *J. Cell Biol.* **169**, 425–434 (2005).
9. Melendez, A. *et al.* Autophagy genes are essential for dauer development and life-span extension in *C. elegans*. *Science* **301**, 1387–1391 (2003).
10. Juhasz, G., Csikos, G., Sinka, R., Erdelyi, M. & Sass, M. The *Drosophila* homolog of Aut1 is essential for autophagy and development. *FEBS Lett.* **543**, 154–158 (2003).
11. Paludan, C. *et al.* Endogenous MHC class II processing of a viral nuclear antigen after autophagy. *Science* **307**, 593–596 (2005).
12. Nakagawa, I. *et al.* Autophagy defends cells against invading group A *Streptococcus*. *Science* **306**, 1037–1040 (2004).
13. Gutierrez, M. G. *et al.* Autophagy is a defense mechanism inhibiting BCG and *Mycobacterium tuberculosis* survival in infected macrophages. *Cell* **119**, 753–766 (2004).
14. Betz, U. A., Vosshenrich, C. A., Rajewsky, K. & Muller, W. Bypass of lethality with mosaic mice generated by Cre–*loxP*-mediated recombination. *Curr. Biol.* **6**, 1307–1316 (1996).
15. Ohsumi, Y. Molecular dissection of autophagy: two ubiquitin-like systems. *Nature Rev. Mol. Cell Biol.* **2**, 211–216 (2001).
16. Kabeya, Y. *et al.* LC3, a mammalian homologue of yeast Apg8p, is localized in autophagosome membranes after processing. *EMBO J.* **19**, 5720–5728 (2000).
17. Ciechanover, A. & Brundin, P. The ubiquitin proteasome system in neurodegenerative diseases: sometimes the chicken, sometimes the egg. *Neuron* **40**, 427–446 (2003).
18. Bossy-Wetzel, E., Schwarzenbacher, R. & Lipton, S. A. Molecular pathways to neurodegeneration. *Nature Med.* **10** (Suppl.), S2–S9 (2004).
19. Bence, N. F., Sampat, R. M. & Kopito, R. R. Impairment of the ubiquitin–proteasome system by protein aggregation. *Science* **292**, 1552–1555 (2001).
20. Yu, W. H. *et al.* Macroautophagy–a novel β-amyloid peptide-generating pathway activated in Alzheimer's disease. *J. Cell Biol.* **171**, 87–98 (2005).
21. Tanaka, Y. *et al.* Accumulation of autophagic vacuoles and cardiomyopathy in LAMP-2-deficient mice. *Nature* **406**, 902–906 (2000).
22. Nishino, I. *et al.* Primary LAMP-2 deficiency causes X-linked vacuolar cardiomyopathy and myopathy (Danon disease). *Nature* **406**, 906–910 (2000).
23. Webb, J. L., Ravikumar, B., Atkins, J., Skepper, J. N. & Rubinsztein, D. C. α-Synuclein is degraded by both autophagy and the proteasome. *J. Biol. Chem.* **278**, 25009–25013 (2003).
24. Ravikumar, B. *et al.* Inhibition of mTOR induces autophagy and reduces toxicity of polyglutamine expansions in fly and mouse models of Huntington disease. *Nature Genet.* **36**, 585–595 (2004).
25. Fortun, J., Dunn, W. A. Jr, Joy, S., Li, J. & Notterpek, L. Emerging role for autophagy in the removal of aggresomes in Schwann cells. *J. Neurosci.* **23**, 10672–10680 (2003).
26. Levine, B. & Yuan, J. Autophagy in cell death: an innocent convict? *J. Clin. Invest.* **115**, 2679–2688 (2005).
27. Bontekoe, C. J. *et al.* Knockout mouse model for *Fxr2*: a model for mental retardation. *Hum. Mol. Genet.* **11**, 487–498 (2002).
28. Koike, M. *et al.* Involvement of two different cell death pathways in retinal atrophy of cathepsin D-deficient mice. *Mol. Cell. Neurosci.* **22**, 146–161 (2003).
29. Waguri, S. *et al.* Cysteine proteinases in GH4C1 cells, a rat pituitary tumour cell line, are secreted by the constitutive and regulated secretory pathways. *Eur. J. Cell Biol.* **67**, 308–318 (1995).
30. Tanahashi, N. *et al.* Hybrid proteasomes. Induction by interferon-γ and contribution to ATP-dependent proteolysis. *J. Biol. Chem.* **275**, 14336–14345 (2000).

Supplementary Information is linked to the online version of the paper at www.nature.com/nature.

Acknowledgements We thank T. Kaneko, T. Kouno and K. Tatsumi for technical assistance. We also thank A. Yabashi, K. Kanno, F. Kaji and K. Ikeue for help with morphological analysis, J. Ezaki for discussion, and Z. Yue for critical reading of the manuscript. This work was supported in part by a Grant-in-Aid from the Ministry of Education, Culture, Sports, Science and Technology of Japan.

Author contributions M.K. and T.C. generated *Atg7*$^{flox/flox}$ mice, and M.K. and J.I. performed most of the experiments to characterize *Atg7*$^{flox/flox}$; nestin-*Cre* mice. S.W. performed histological and microscopic analyses, and S.M. performed the biochemical analysis of proteasome activity. M.K., S.W. and K.T. wrote the paper. All authors discussed the results and commented on the manuscript.

Author Information Reprints and permissions information is available at npg.nature.com/reprintsandpermissions. The authors declare no competing financial interests. Correspondence and requests for materials should be addressed to K.T. (tanakak@rinshoken.or.jp).